NASA Technical Paper 2102

February 1983

A Potential-Energy Scaling Model To Simulate the Initial Stages of Thin-Film Growth

J. H. Heinbockel,
R. A. Outlaw,
and G. H. Walker

NASA

NASA
Technical
Paper
2102

1983

A Potential-Energy Scaling Model To Simulate the Initial Stages of Thin-Film Growth

J. H. Heinbockel
Old Dominion University
Norfolk, Virginia

R. A. Outlaw
and G. H. Walker
Langley Research Center
Hampton, Virginia

NASA
National Aeronautics
and Space Administration

**Scientific and Technical
Information Branch**

INTRODUCTION

The need to develop large solar-cell arrays for space applications has stimulated a great interest in thin-film photovoltaics because of their projected high power-to-weight ratio (greater than 1 kW/kg). Specifically, it would be advantageous to develop cost-effective thin-film GaAs solar cells because they possess a wide range of desirable characteristics for space applications (ref. 1). Such cells could be launched and deployed by the Space Shuttle as solar arrays to be used as long-term power supplies for various Shuttle- and satellite-related missions.

A promising approach for developing these solar cells is to epitaxially grow high-efficiency photovoltaic thin films on low-weight, inexpensive foreign substrates using vapor deposition techniques. In order to construct high-efficiency solar cells, it is necessary to produce well-ordered, defect-free GaAs epitaxial films. The degree of crystalline order achieved will be controlled by the adsorption, nucleation, and lateral-growth behavior in the first few layers deposited. This behavior is, in turn, controlled by such parameters as the deposition rate, surface temperature, adatom mobility, adatom-substrate chemical reactivity, surface defect density, and lattice registry of the system. In order to assess the relative sensitivity of these parameters and to model experimental research efforts, a solid-on-solid (SOS) Monte Carlo computer simulation for a one-component system is presented that utilizes a potential-energy scaling technique over a 400-site array.

Although numerous Monte Carlo models exist (refs. 2 to 5), the advantage of this approach is that it allows single events to occur simultaneously at all sites of the array within the constraints of the surrounding potential-energy field and the thermal fluctuations associated with a given substrate temperature. This is in contrast to past models, which utilized rate equations to determine multiple events for a given atom (in one sampling interval) while freezing the motions of all other atoms in the array. Continuous updating of the potential energy over all sites of the array on a time scale sufficiently small to cover single events at each site (e.g., adsorption/desorption of atoms and single-atom jumps to neighboring sites) is made possible by the use of ordered statistics. Therefore, the simultaneous changes at all sites and the resulting individual atomic interactions provide the conditions necessary to simulate thin-film growth in a near physically real manner.

MODEL CONCEPTS

The model employs a 20 × 20 square array with periodic boundary conditions as the substrate (and reference plane) on which atoms are deposited. As atoms are randomly added to the sites they are free to desorb, migrate, diffuse into (incorporate) and out of the substrate, or remain localized. These changes alter the stacking height of each column growing on a particular site, and also change the potential energy at that site and at neighboring sites. Figure 1 illustrates a typical surface topography (terrace-ledge-kink) and represents the surface model used for the solid-on-solid (SOS) method of studying crystal growth. In this approach, atoms are represented by cubes and are constrained to grow in well-defined columns.

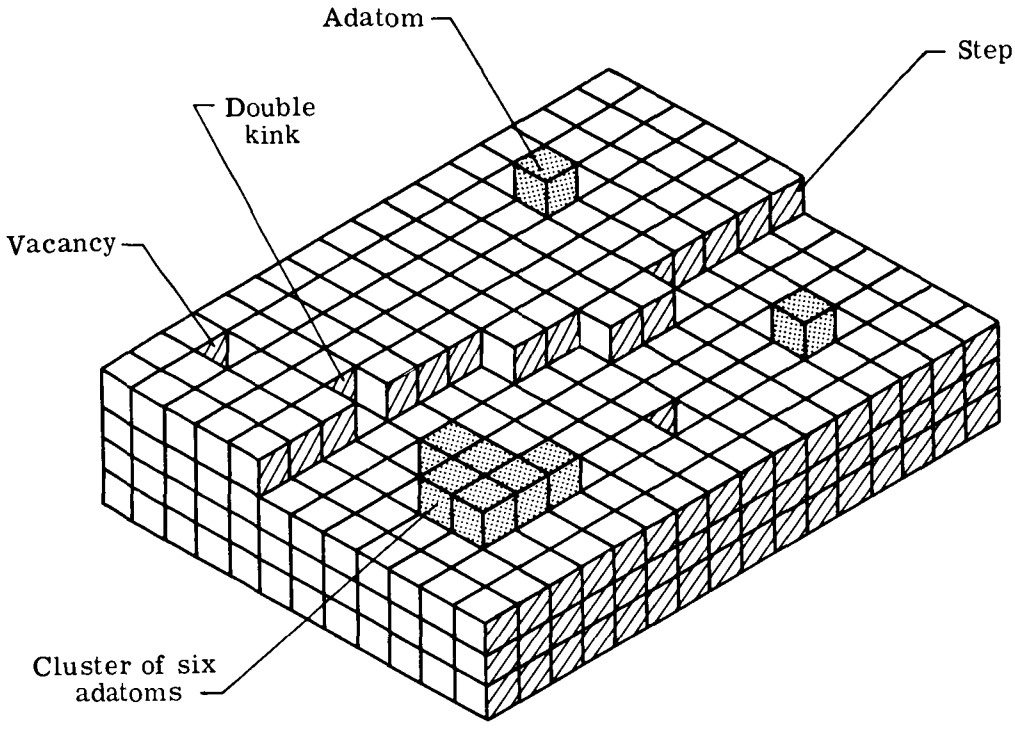

Figure 1.- Geometry of terrace-ledge-kink SOS model.

The physical constraints that determine the temporal behavior of every atom located at the surface of each column site (i,j) are based on the interaction potential of each surface atom relative to the substrate and to its nearest neighbors. The interaction potential across a perfectly homogeneous surface with well depth U_o and interatomic distance a_o is depicted as changing uniformly from site to site (fig. 2(a)). (The symbols used in this paper are defined in a list after the references.) A typical interaction potential across a heterogeneous surface is shown in figure 2(b). The variation in potential energy at different sites reflects the many surface features shown in figure 1, such as vacancies, steps, kinks, and clusters of various sizes. In this model it is assumed that all incident atoms adsorbed on the surface thermally accommodate to the surface instantly. The sticking coefficient S for the substrate and the growing film is governed by

$$S = S_o(1 - \theta)^{\xi} \tag{1}$$

where θ is the coverage S_o is the sticking coefficient at zero coverage and ξ is the order of bonding.

Once an atom is adsorbed onto, or migrates to, a particular site (i,j), the potential interaction energy at that site immediately changes from that of the atom below to that of the newly adsorbed atom. If an atom is desorbed or migrates away, the potential at that site changes to represent the atom that was immediately below it, that is, the "new surface atom." Since the heat of adsorption at zero coverage reflects the number of bonds that an adsorbed atom makes with the substrate (e.g., three bonds for (111) face-centered cubic (fcc) structure, four bonds for (100) fcc, and five bonds for (110) fcc), only the lateral interactions of the growing first

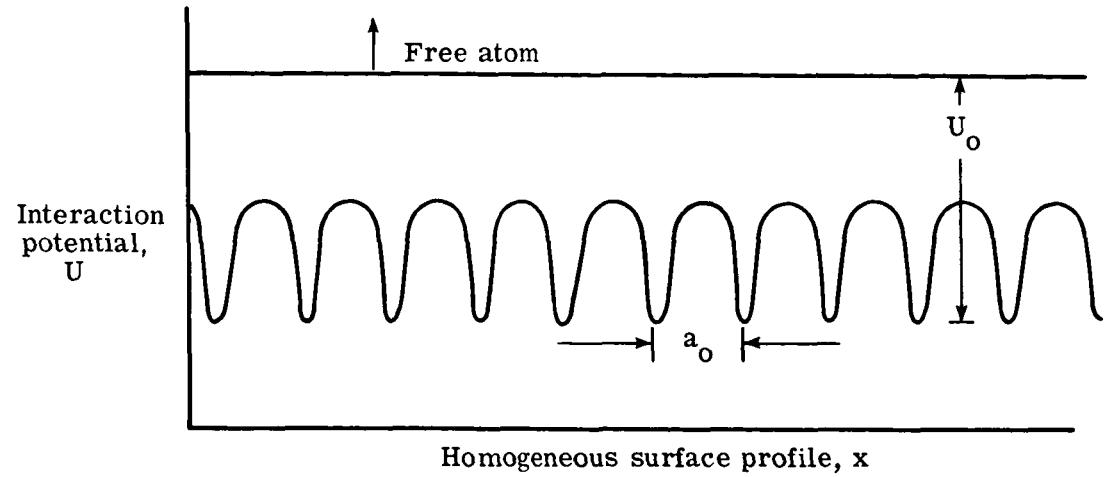

(a) Variation over a uniform homogeneous surface.

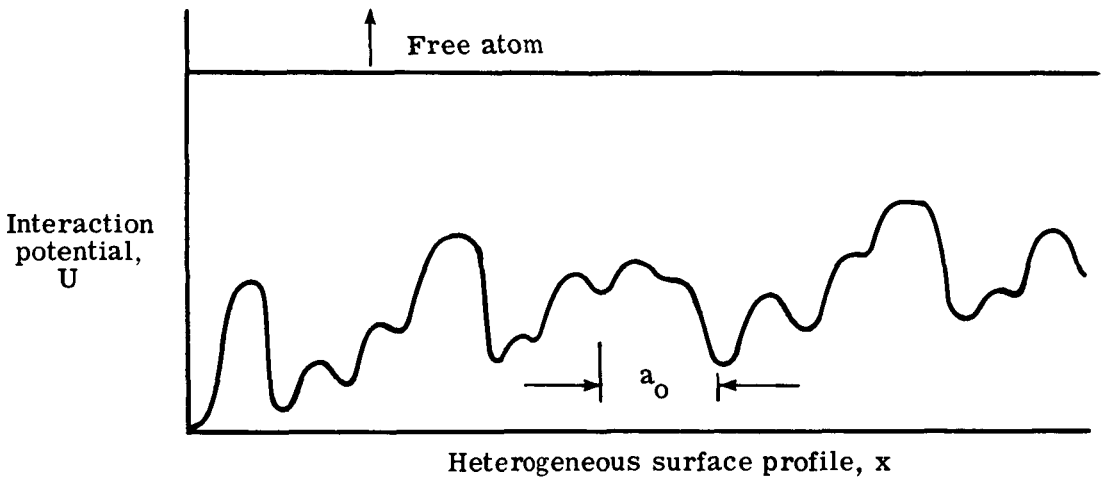

(b) Disturbances in surface potential caused by vacancies, dislocations, kinks, and impurities.

Figure 2.- Variations in potential energy at surface.

layer need to be considered individually. In addition, the changes in potential energy at a particular site will affect the potential energy of the nearest neighbors, second-nearest neighbors, and third-nearest neighbors in the first layer of growth. Updating the potential energy at a given site following a kinetic event therefore requires simultaneous updating of the potential energy for all surrounding sites.

The changes in potential energy that occur along a lineal section of a homogeneous surface upon the adsorption of a single adatom at site (i,j) are shown in figure 3. Note that the potential at that site increases by an amount ϕ_o, and the potential at adjacent sites decreases by an incremental amount α. This represents

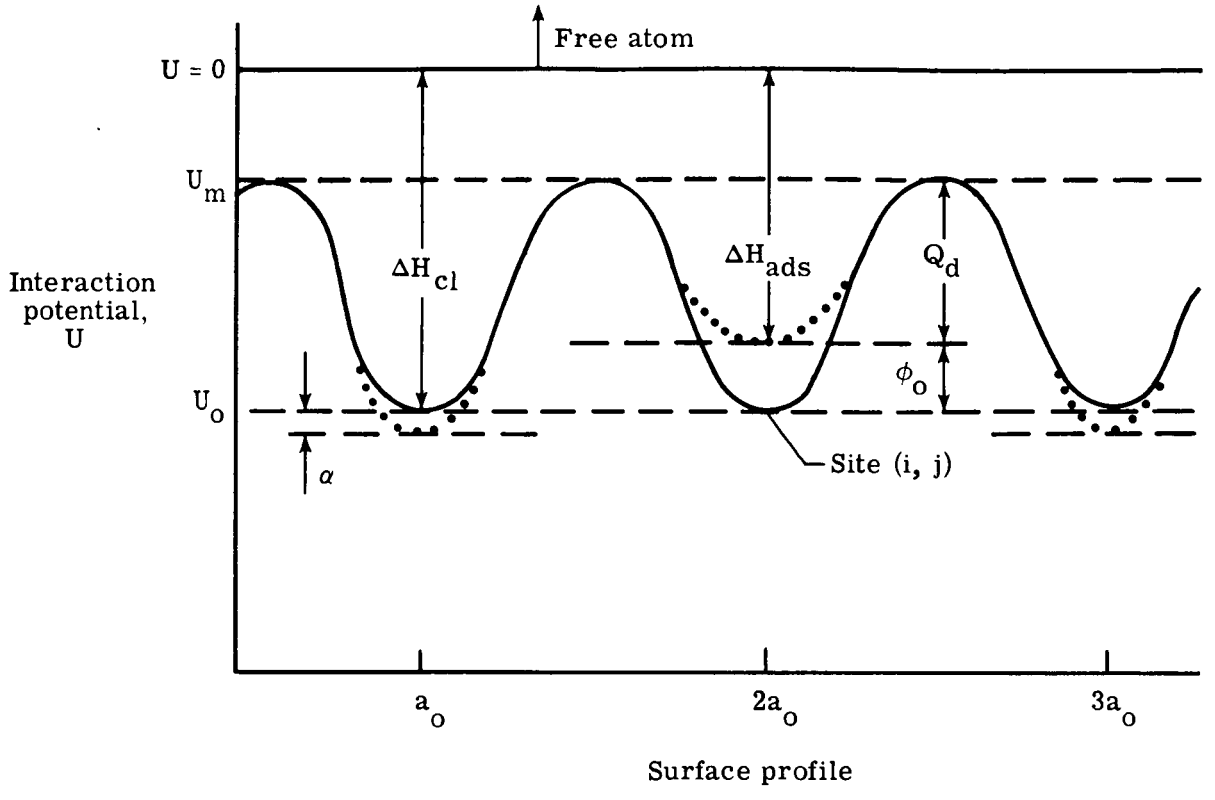

Figure 3.- Changes in potential energy along lineal section of a homogeneous surface upon adsorption of a single adatom at site (i,j).

the actual physical condition of the particular adatom at site (i,j); it requires less energy to desorb or migrate than did the original surface atom at that site when it was surrounded by all its nearest neighbors. Further, the deeper potential at the neighboring sites reflects the increased energy necessary to desorb an atom at those sites. This is a result of the increase in number of neighbors for those sites.

Figure 4 shows the variation in potential energy at site (i,j) as lateral neighbors are progressively added. For each nearest neighbor, a potential-energy increment α is subtracted, and increments of β and γ are subtracted for second and third neighbors, respectively. Autoepitaxy requires that the initial potential U_o $\left(U_o \equiv \Delta H_{cl}\right)$ be recovered when all the surrounding-neighbor sites have been filled. Thus, for an adatom at site (i,j),

$$U(i,j) = -U_o + \phi_o = -\Delta H_{ads} \tag{2}$$

For a (110) fcc surface, the addition of two nearest neighbors (-2α), two second-nearest neighbors (-2β), and four third-nearest neighbors (-4γ) to the adatom recovers the potential of the original site. Since

$$\phi_o = 2\alpha + 2\beta + 4\gamma$$

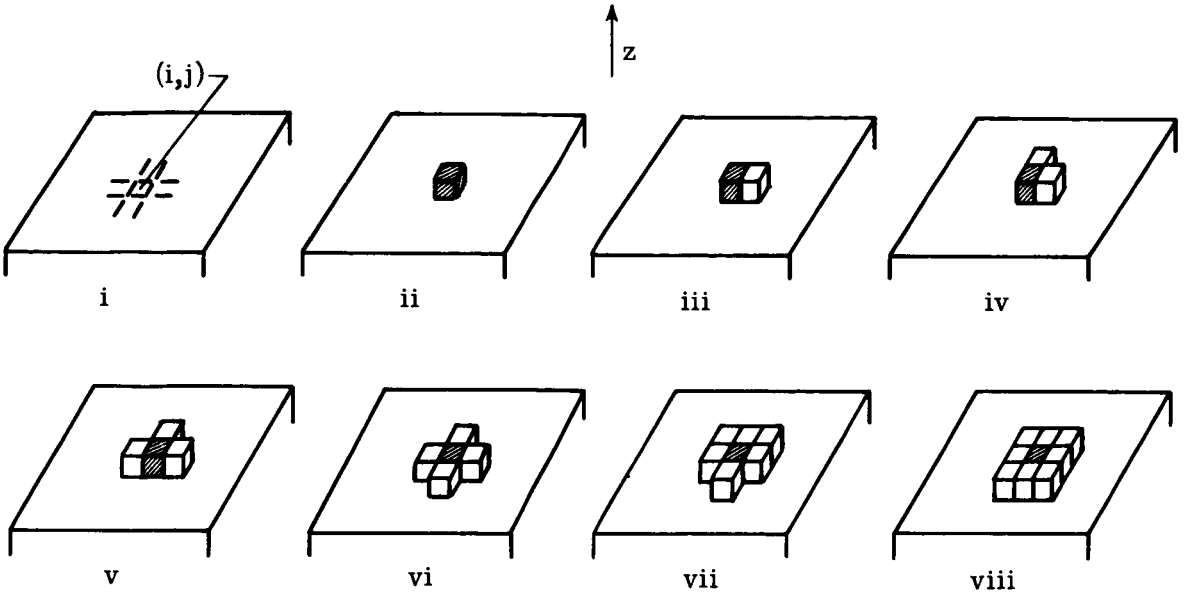

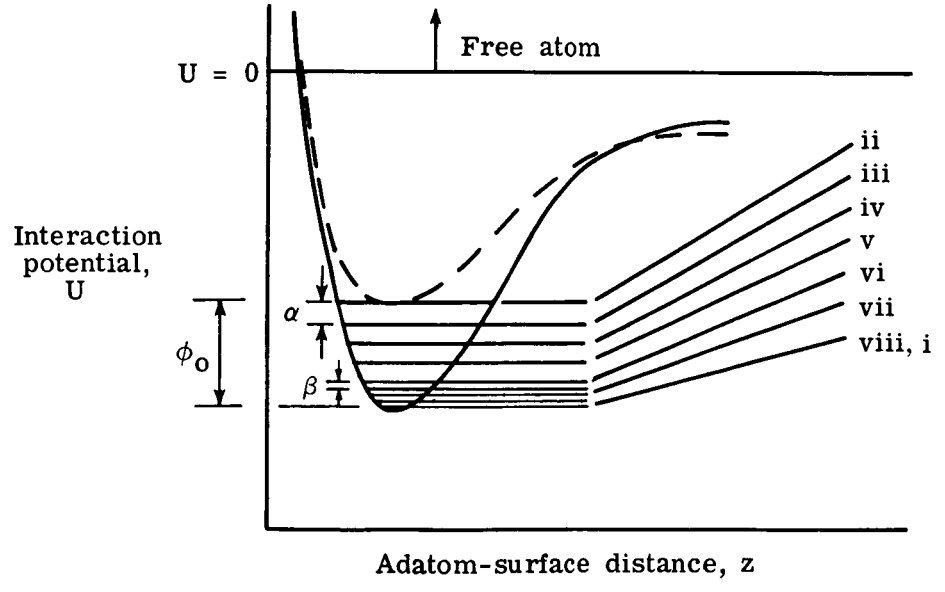

Figure 4.- Variation in potential energy at site (i,j) as lateral neighbors are progressively added.

then

$$U(i,j) = -U_o + \phi_o - 2\alpha - 2\beta - 4\gamma = -U_o$$

The values of α, β, and γ are determined by the lateral bond strength of a particular system.

Energy Fluctuations and Potential Scaling

The behavior at each site in the entire array is monitored once during every sampling interval Δt_s. By random-number generation, the fluctuation in vibrational (thermal) energy ε is added to the interaction potential $U(i,j)$ at each site, and the resulting total energy $E(i,j)$ for the site is compared with the magnitude of the energy barriers for desorption, surface migration, incorporation, and diffusion of a substrate atom into the film. If $E(i,j)$ of the atom exceeds one of these barriers but is less than another, then the atom moves accordingly. If $E(i,j)$ is less than the lowest barrier, then the atom remains localized. For each sampling interval Δt_s, an atom in an arbitrary site (i,j) has the total energy

$$E(i,j) = U(i,j) + \varepsilon \tag{3}$$

where ε is determined by random number R from the Boltzmann distribution

$$f(\varepsilon) = \lambda \exp(-\lambda\varepsilon) \qquad (\varepsilon > 0) \tag{4}$$

where $\lambda = 1/kT$. The mean energy of this distribution is

$$\langle\varepsilon\rangle = \int_0^\infty \varepsilon\, f(\varepsilon)\, d\varepsilon = kT = \frac{1}{\lambda} \tag{5}$$

and the cumulative energy distribution is given by

$$F(\varepsilon) = \int_0^\varepsilon f(\varepsilon)\, d\varepsilon = 1 - \exp(-\lambda\varepsilon) \tag{6}$$

A random variate ε can be generated by using the inverse function associated with the cumulative distribution (ref. 6). Thus, for the uniform random number R between 0 and 1 and with $R = F(\varepsilon)$, the inverse function gives the random energy

$$\varepsilon = -kT \ln(1 - R) \tag{7}$$

Equation (1) then becomes

$$E(i,j) = U(i,j) - kT \ln(1 - R) \tag{8}$$

Selection of a random number during each Δt_s allows a value $E(i,j)$ to be determined. Figure 5 represents the ground state potential-energy scale for the adsorbate atoms, to which $E(i,j)$ is compared. Basically, four cases are considered.

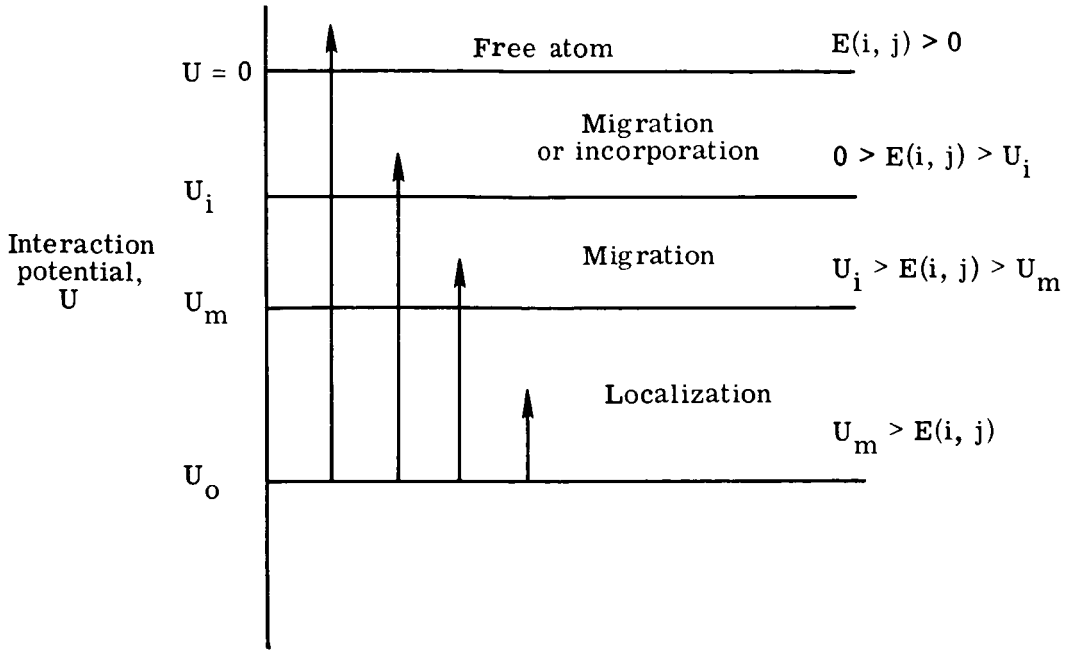

Figure 5.- Total energy of site (i,j) at a given instant compared with threshold levels of atomic events.

1. If $E(i,j) > 0$, then the atom desorbs and disappears from the surface.

2. If $0 > E(i,j) > U_i$, then the atom migrates or is incorporated into the bulk and disappears from the surface.

3. If $U_i > E(i,j) > U_m$, then the atom migrates to a vacant nearest-neighbor position.

4. If $U_m > E(i,j)$, then the atom remains localized.

In the first case, the desorbing atom vacates the site and is no longer monitored. The frequency of desorption ν_{des} is dependent on the number of bonds to other atoms in the surface and is given by (ref. 5)

$$\nu_{des} = \frac{1}{\tau_o} \exp\left(-\frac{\eta\phi}{kT}\right) \tag{9}$$

where η is the number of bonds, ϕ is the single-bond energy, and τ_o is the vibrational period of surface atoms ($\tau_o \approx 10^{-12}$ sec).

In the second case, if an atom has sufficient energy to incorporate then it also has sufficient energy to migrate. Whether it will incorporate or migrate depends on the relative probability of each possibility. In the case of migration, the availability of more than one site for migration is determined by the coordination number associated with the available sites. The higher the coordination number of an available site, the deeper the potential well and the smaller the energy barrier to

migration. This increases the probability of migration to that site. The experimental evidence to support this assumed behavior is sizeable (ref. 7).

Migration, or surface diffusion, can be localized or nonlocalized, depending on the amount of thermal energy absorbed. The case of localized adatom diffusion is represented by (ref. 8) where a_o is the interatomic distance (ℓ = 1/4 for

$$D = \frac{\ell a_o^2}{\tau_o} \exp\left(-\frac{Q_d}{kT}\right) \tag{10}$$

a (100) fcc structure) and Q_d is the energy of migration. (See fig. 3.) An adatom in this state can be characterized by three degrees of freedom, two vibrational and one translational, and moves over single saddle points. If the adatom has significantly more energy than Q_d but less than the desorption energy, then nonlocalized diffusion will occur. The atom is then characterized by one vibrational and two translational degrees of freedom. In this case, the atom may take several hops along potential-energy saddle point paths, or it may leap completely over the top of a nearest-neighbor atom. In general, the Q_d obtained from experiments probably represents some combination of localized and nonlocalized diffusion.

In the case of incorporation, an atom is considered to have been removed from the surface in the same way that an adatom desorbs. It is assumed that the bulk vacancy concentration is sufficient to receive the adatoms, and thus the atom simply disappears from the surface site. The defining equation for the diffusion of atoms from the adlayer (adsorption layer) into the bulk is (ref. 9)

$$c_b(z,t) = \frac{R_d t}{\delta}\left[1 + \frac{z^2}{2Dt}\,\mathrm{erfc}\left(\frac{z}{2Dt}\right) - \frac{z}{\pi Dt}\exp\left(\frac{-z^2}{4Dt}\right)\right] \tag{11}$$

where c_b is the bulk concentration in the selvedge, R_d is the deposition rate, and erfc is the error function complement. The amount Δc_s incorporated, then, is the total amount absorbed by the bulk per unit area, as follows:

$$\Delta c_s = -\int_0^t D\left(\frac{\partial c_b}{\partial z}\right)_{z=0} dt = \frac{4}{3}\left(\frac{R_d t}{\delta}\right)\left(\frac{Dt}{\pi}\right)^{1/2} \tag{12}$$

In the third case, the atom has only enough energy to migrate. Surface migration is treated as desorption followed by adsorption at a neighboring site. In the fourth case, no change occurs at the site.

Initially, similar determinations must be made for each adatom that adsorbs onto a substrate of a different species. These determinations are made by replacing $E(i,j)$ with $E_s(i,j)$ in the inequality argument presented previously. Each interaction is considered separately until all substrate sites are covered.

After the substrate is completely covered by the adlayer, diffusion of substrate atoms through the growing film to the surface can be approximated by randomly depositing substrate atoms onto surface vacancy sites at a rate controlled by the diffusion equations for the adlayer-substrate system. Since the growing film is so thin,

this can be considered diffusion through a membrane, and the total number of substrate atoms emerging at the surface can be calculated by (ref. 9)

$$(\Delta c_s)_{sub} = \frac{Dc_b}{\delta}\left(t - \frac{\delta^2}{6D}\right) \tag{13}$$

Ordered Statistics

The residence time or stay time, of an atom on a surface is given by the Frenkel equation

$$\tau = \tau_o \exp\left(-\lambda \Delta H_{ads}\right) \tag{14}$$

where ΔH_{ads} is the heat of adsorption and τ_o is the period of vibration for surface atoms ($\tau_o \approx 10^{-12}$ sec). (It is assumed here that $\Delta H_{ads} = \Delta H_{des}$.) Ideally, then, the most physically real sampling time that corresponds to changes in vibrational energy, and therefore to changes in $E(i,j)$, is $\Delta t_s = \tau_o$. Computer costs, of course, prohibit the extensive run times that would be required to sample 400 sites 10^{12} times each second. In order to circumvent this difficulty, the method of ordered statistics is applied (ref. 6). Essentially, most of the time-dependent energy variation at a particular site results in insufficient thermal fluctuation for atomic movement, so the atoms are localized over most of the sampling interval. This large time interval of atomic localization is not important to the actual thin-film growth because there are no atom movements; therefore, only the fraction of the sampling interval in which movement does occur needs to be considered. Thus, we must determine what fraction of the time the site energy is in excess of the minimum activation barrier for movement.

Let $\varepsilon 1, \varepsilon 2, \ldots, \varepsilon n$ denote n random samples from the exponential distribution in equation (4) and let $\varepsilon_{(1)}, \varepsilon_{(2)}, \ldots, \varepsilon_{(n)}$ denote the ordered arrangement (from low to high) of the n random samples with $\varepsilon_{(i-1)} < \varepsilon_{(i)}$ for all $i = 2, 3, \ldots, n$ and $\varepsilon_{(n)} = \max(\varepsilon 1, \varepsilon 2, \ldots, \varepsilon n)$. The probability distribution of the largest ordered statistic $\varepsilon = \varepsilon_{(n)}$ is given by

$$g(\varepsilon) = n[F(\varepsilon)]^{n-1} f(\varepsilon) \qquad (0 < \varepsilon < \infty) \tag{15}$$

where $f(\varepsilon)$ and $F(\varepsilon)$ are given by equations (4) and (6).

Figure 6 presents examples of this distribution for a temperature of 500 K and different sampling sizes ($n = 10^7$, 10^8, and 10^9). The cumulative frequency distribution is given by

$$G(\varepsilon_o) = P(\varepsilon < \varepsilon_o) = \int_0^{\varepsilon_o} g(\varepsilon)\, d\varepsilon = \left[1 - \exp(-\lambda \varepsilon_o)\right]^n \tag{16}$$

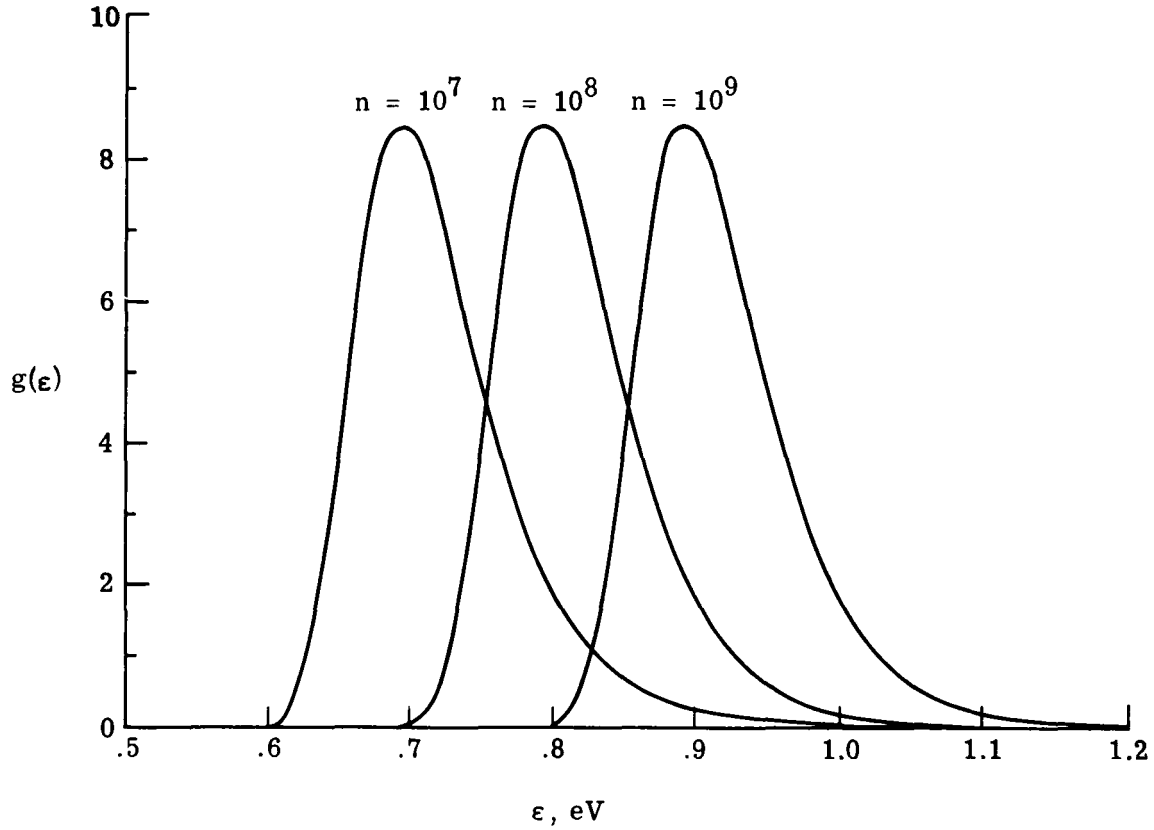

Figure 6.- Distribution function of Boltzmann-ordered statistics at T = 500 K for different values of the sampling interval.

To generate random variables $\varepsilon_{(n)}$ from this distribution, a uniform random number R is generated such that $G\left[\varepsilon_{(n)}\right] = R$. This gives

$$\varepsilon_{(n)} = -kT \ln(1 - R^{1/n}) \qquad (0 < R < 1) \tag{17}$$

which can be compared with equation (6). Note that for very large n, we can approximate $\varepsilon_{(n)}$ by

$$\varepsilon_{(n)} = -kT \ln\left(-\frac{1}{n} \ln R\right) \tag{18}$$

If, for example, T = 500 K, Q_d = 0.7 eV, and the average mean time between hops is $\tau_d = 10^{-12} \exp(\lambda Q_d) = 10^{-5}$ sec, then in a sampling interval of $\Delta t_s = 10^{-5}$ sec, a single hop occurs. Any smaller sampling interval is unnecessary because no movement occurs. Any larger sampling interval (i.e., greater than multiples of 10^{-5} sec) would result in multiple events for a single atom and multiple events at other sites in the array. Therefore, the more the sampling interval exceeds the time of a single event, the less physically real the model becomes.

After selecting a particular system for adsorption, the minimum activation barrier determines the sampling interval and therefore the number of random samples n.

The ordered statistic $\varepsilon_{(n)}$ can be determined by a random-number generator and equation (17). Combining equations (17) and (3) gives the total energy at site (i,j) as

$$E(i,j) = U(i,j) - kT \ln\left(1 - R^{1/n}\right) \tag{19}$$

The same procedure described previously to determine atomic events is then followed.

PROCEDURE

The changes in potential energy over a uniform face-centered cubic surface can be depicted by a mnemonic mask. When the center of this mask is placed over site (i,j), the mask characterizes the changes in potential energy that occur both at the central site and at the nearest-neighbor sites upon the adsorption of an atom. As shown in figure 3, the adsorption of an adatom at site (i,j) drives the potential energy at that site positive by an amount ϕ_o and simultaneously drives the potential at the nearest-neighbor sites more negative. As other adatoms arrive at nearest-neighbor sites, the potential at site (i,j) incrementally becomes more negative. In the case of a (100) fcc surface, there are four nearest neighbors (incremental change α) and four second-nearest neighbors (incremental change β) in the surface layer. As these sites are filled, the potential at site (i,j) returns to U_o. Thus, for the different crystal faces

$$\phi_o = 4\alpha + 4\beta \qquad \left(\alpha = \alpha\left(\frac{\sqrt{2}}{2} a_o\right);\quad \beta = \beta(a_o)\right) \tag{20}$$

for (100) fcc surface,

$$\phi_o = 6\alpha' + 6\beta' \qquad \left(\alpha' = \alpha\left(\frac{\sqrt{2}}{2} a_o\right);\quad \beta' = \beta\left(\frac{\sqrt{3}}{2} a_o\right)\right) \tag{21}$$

for (111) fcc surface, and

$$\phi_o = 2\alpha'' + 2\beta'' + 4\gamma \qquad \left(\alpha'' = \alpha(a_o);\quad \beta'' = \beta\left(\sqrt{2}a_o\right);\quad \gamma = \gamma\left(\sqrt{3}a_o\right)\right) \tag{22}$$

for (110) fcc surface.

Figure 7 gives the actual atomic arrangement for the three low-index crystal faces for a face-centered cubic structure, and shows how the potential-energy increments are considered in terms of the SOS model. The potential at each site is assessed independently by moving the mnemonic mask to the site and evaluating all the positions on the mask to determine the new potential. This ultimately determines whether an atom has been added, lost, or unchanged since the last survey. In the case of atoms in a crystal that are bonded by van der Waal's forces, the effects of second- and third-nearest neighbors are quite significant, but for metal, ionic, and covalent bonds, only the primary bonds need to be considered ($\beta = \gamma = 0$). The (110) face, however, is an exception ($\gamma = 0$).

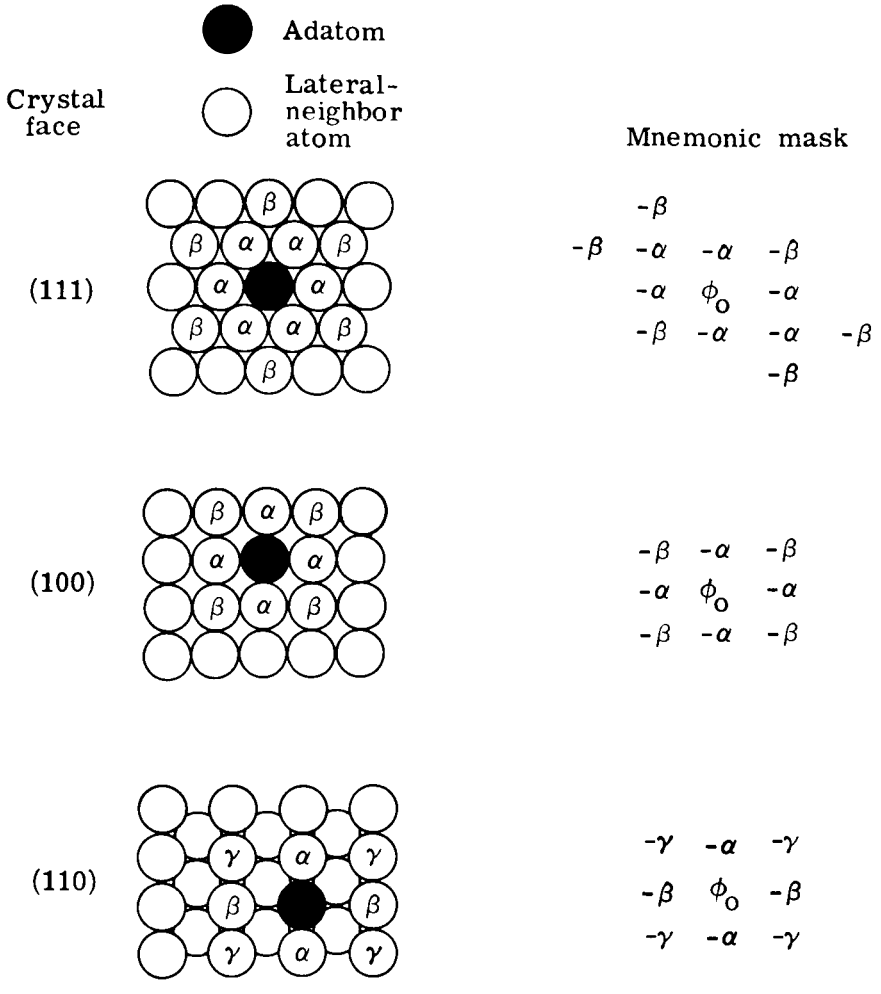

Figure 7.- Mnemonic mask used to update potentials at site (i,j) and neighboring sites following the motion of an atom.

The flow chart for this simulation is presented in figure 8. Initially, the boundary conditions can be established by adjusting the site potentials to reflect desired distributions of kink sites, ledges, impurities, or other defects. Any degree of heterogeneity can be included. Ordinarily, an assumed impingement flux R_d dictates the number of adatoms arriving at the surface during a prescribed sampling interval. Depending on the value of S, adatoms are added to sites by random-number generation, and the mnemonic mask is then used to update the potential energy at each site as well as that at each of its surrounding neighbors. Every site in the array is surveyed, and a random thermal energy $\varepsilon(R)$ is generated and ultimately used to determine the total energy at site (i,j). (See eq. (19).) For each site it is then determined whether desorption, migration, incorporation, or localization has occurred, and the atom is moved accordingly. Ultimately, all the sites are independently and randomly sampled. This interaction procedure is followed until the desired growth time has expired. At this point, crystal growth measures such as vertical growth rate, surface diffusion coefficient, desorption rate, incorporation rate, nucleation rate, and cluster size distribution can be calculated. Further, graphic displays of surface migration paths and nucleation island growth and coalescence can be plotted, along with isometric views of the growth.

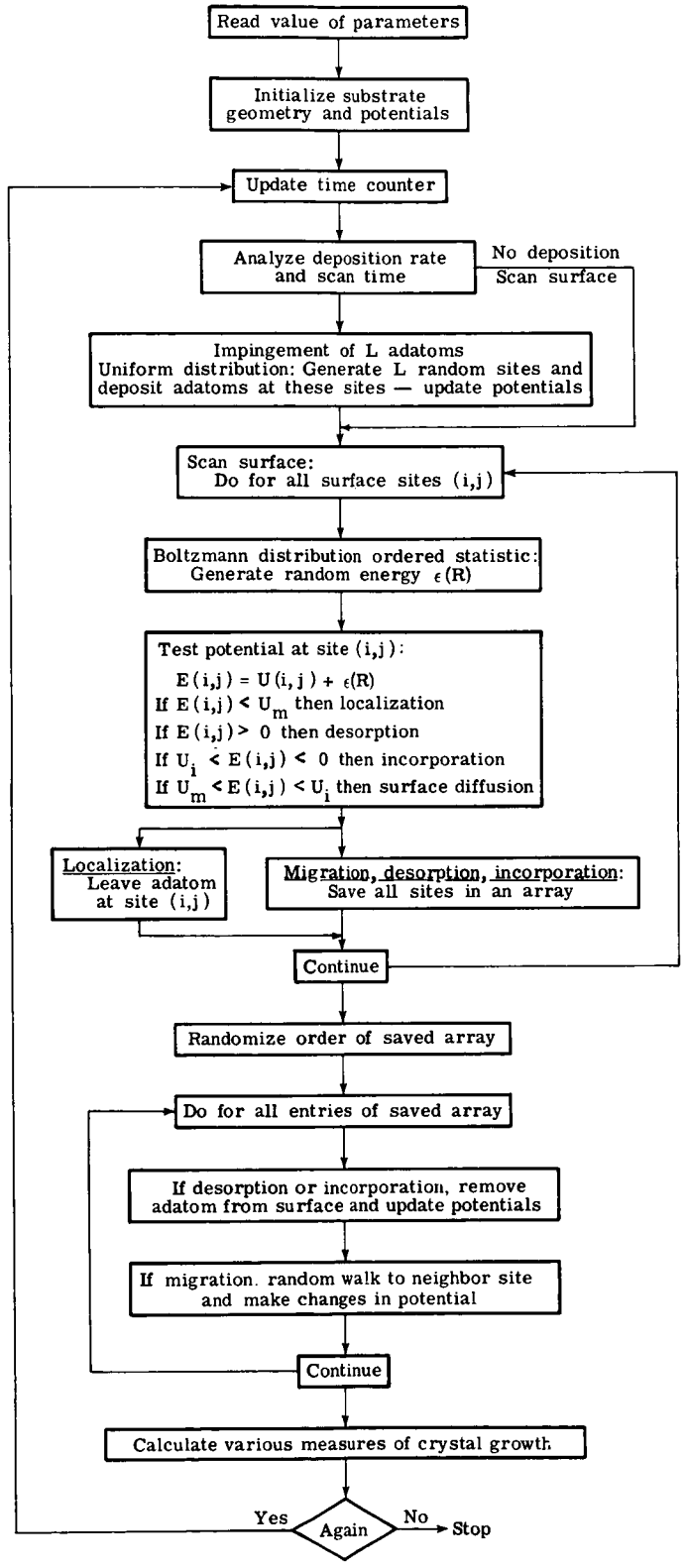

Figure 8.- Flow chart for Monte Carlo SOS computer simulation of thin-film growth.

RESULTS AND DISCUSSION

Five computer experiments were conducted on a (100) fcc surface to assess the physical behavior of the model. The experiments and their parametric variations are summarized in table I. In order to model a thin-film system, several a priori

TABLE I.- MODEL EXPERIMENTS AND PARAMETERS

Experiment	R_d, cm^{-2}-sec^{-1} × 10^{15}	T, K	t, sec	Q_d, eV
1 - Surface diffusion of single adatom	0	300, 400, 500, 600, 700	2	0.7
2 - Clustering of nine dispersed atoms	0	400, 500, 600	2	.7
3 - Thin-film growth with a single defect site	.5	550	2	.7
4 - Thin-film growth with variable deposition rate and substrate temperature	.05, .5, 1, 2.5	300, 400, 500, 600, 700	2, 15	.7
5 - Annealing of thin-film growth	0	500, 600, 700, 800	6	.7

parameters must be specified. Since there are insufficient data on any particular semiconductor-metal thin-film system, nominal parameters were chosen for the experiments. These parameters are presented in table II.

TABLE II.- NOMINAL PARAMETERS

$(\Delta H_{ads})_{\theta=0}$, eV	1.7
ΔH_{cl}, eV	3.87
D_{-z} (self-diffusion into growing film), cm^2-sec^{-1}	7.8 exp(-2.98λ)
D_{-z} (diffusion into substrate), cm^2-sec^{-1}	0.44 exp(-2.09λ)
D_{+z} (substrate atom diffusion through film), cm^2-sec^{-1}	0.13 exp(-1.08λ)
Q_d, eV	0.7
S	1

The growth kinetics are quite sensitive to the magnitudes of these parameters. For example, the selected values for $(\Delta H_{ads})_{\theta=0}$ and Q_d are high, and for moderate to low temperatures this will yield capture-controlled kinetics. For the same temperature range, reducing $(\Delta H_{ads})_{\theta=0}$ by one-half will yield desorption-controlled kinetics. An excellent discussion of this argument can be found in reference 2.

Experiment 1 - Surface Diffusion of Single Adatoms

The random migration of atoms over a perfectly uniform surface (fig. 2(a)) is essentially a random walk to nearest-neighbor sites for the (100) fcc crystal face, which has four primary sites. The number of migrations as a function of time is linear and varies exponentially with temperature. A plot of the calculated diffusion coefficient as a function of inverse temperature is given in figure 9. The linear behavior of the diffusion coefficient follows equation (10), and the slope of the Arrhenius plot yields the activation barrier $Q_d = 0.7$ eV (the input condition). This provides a self-consistent check on the migration physics of the computer model. The average number of migrations for each temperature is given adjacent to each data point in figure 9. In the case of a nonuniform surface, both mean diffusion length and migration frequency would be substantially reduced because of the lower probability of escape from kink sites, steps, and other defects.

Experiment 2 - Clustering of Nine Dispersed Atoms

This experiment demonstrated the clustering of atoms to the most stable configuration. Each atom should ultimately maximize its number of nearest neighbors, thus making $U(i,j)$ more negative and therefore more stable. Ideally, the atoms should interact to form a 3×3 array. The dispersed atoms individually random walk and collide to form dimers, trimers, and finally a nine-atom cluster. Figure 10 presents a graphic sequence of the atom motion as a function of time for a substrate at 600 K. In figure 10(b), many migrations have already occurred and the atoms have formed a monomer, two dimers, and a tetramer. Figure 10(c) shows the effective rotation of the tetramer and the clustering of the two dimers and the monomer. In figures 10(c), 10(d), and 10(e), adequate thermal energy was absorbed to break away a single atom from the tetramer, trimer, and dimer, respectively. Eventually each monomer was captured by the growing cluster. Finally, in figure 10(f), the cluster has reached its most stable state. Cluster growth is believed to occur either by this method of monomer capture or by actual en masse motion of one of the clusters, subsequent collision with another cluster, and reorientation of the atoms to registry with this cluster (ref. 2, chapter 3). In the formulation of this model, no consideration was given to the motion of whole clusters, but, as these experiments show, whole clusters can move by individual atom motion at the periphery of the cluster, which results in the net motion of its center of mass.

Experiment 3 - Thin-Film Growth With a Single Defect Site

A generalized point defect is modeled by assuming that the potentials for the "trap" and its nearest-neighbor sites vary in the lateral and vertical directions and are dependent on layer height. (Potentials return to normal after two layers of growth.) Although it is understood that τ_o will vary in the vicinity of defects, there is no simple means of determining its value near a particular defect. It will therefore be assumed that $\tau_o = 10^{-12}$ sec.

Figure 11 shows the prescribed variation in potential energy at the trap, which is positioned at the center of the 20×20 array. A graphic display of the growth

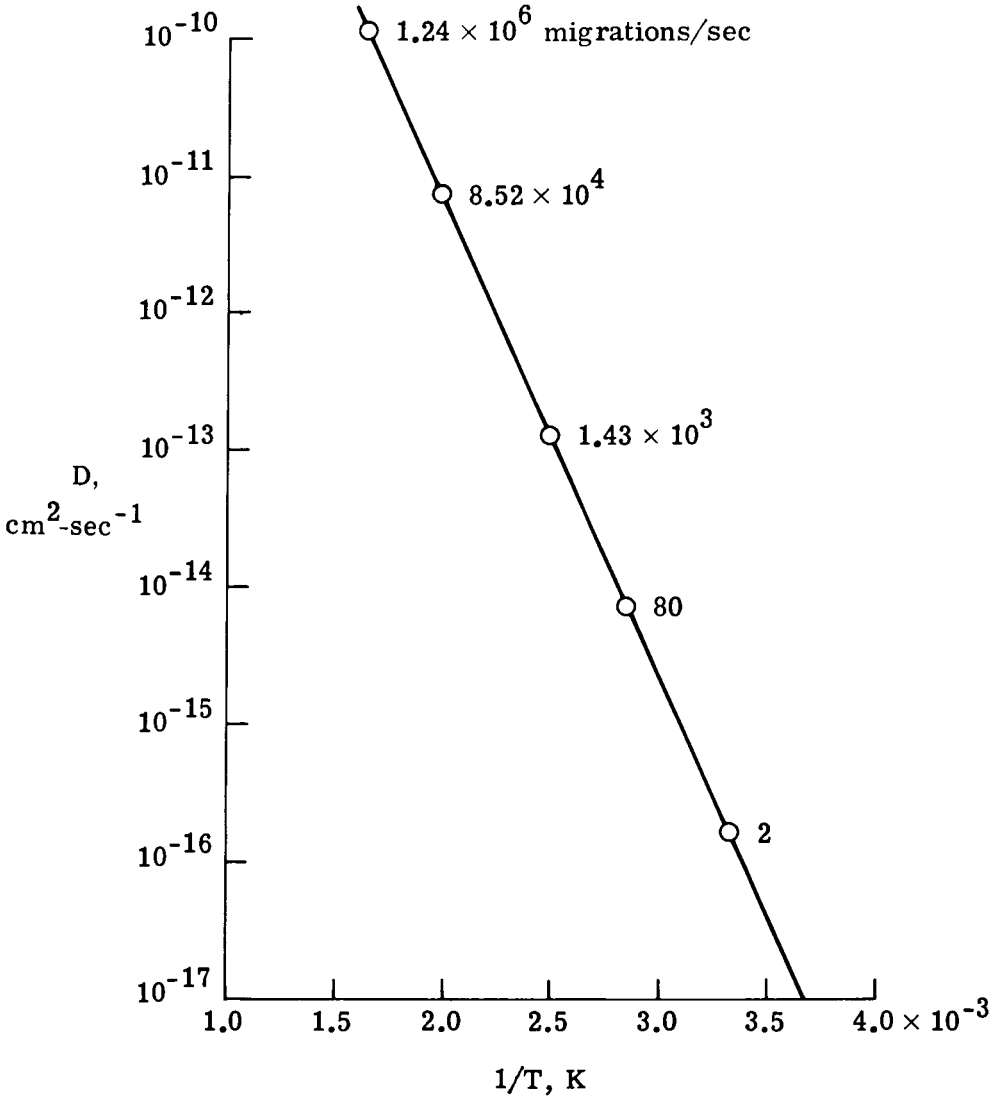

Figure 9.- Arrhenius plot of single-adatom diffusion coefficient over a uniform surface as a function of reciprocal temperature.

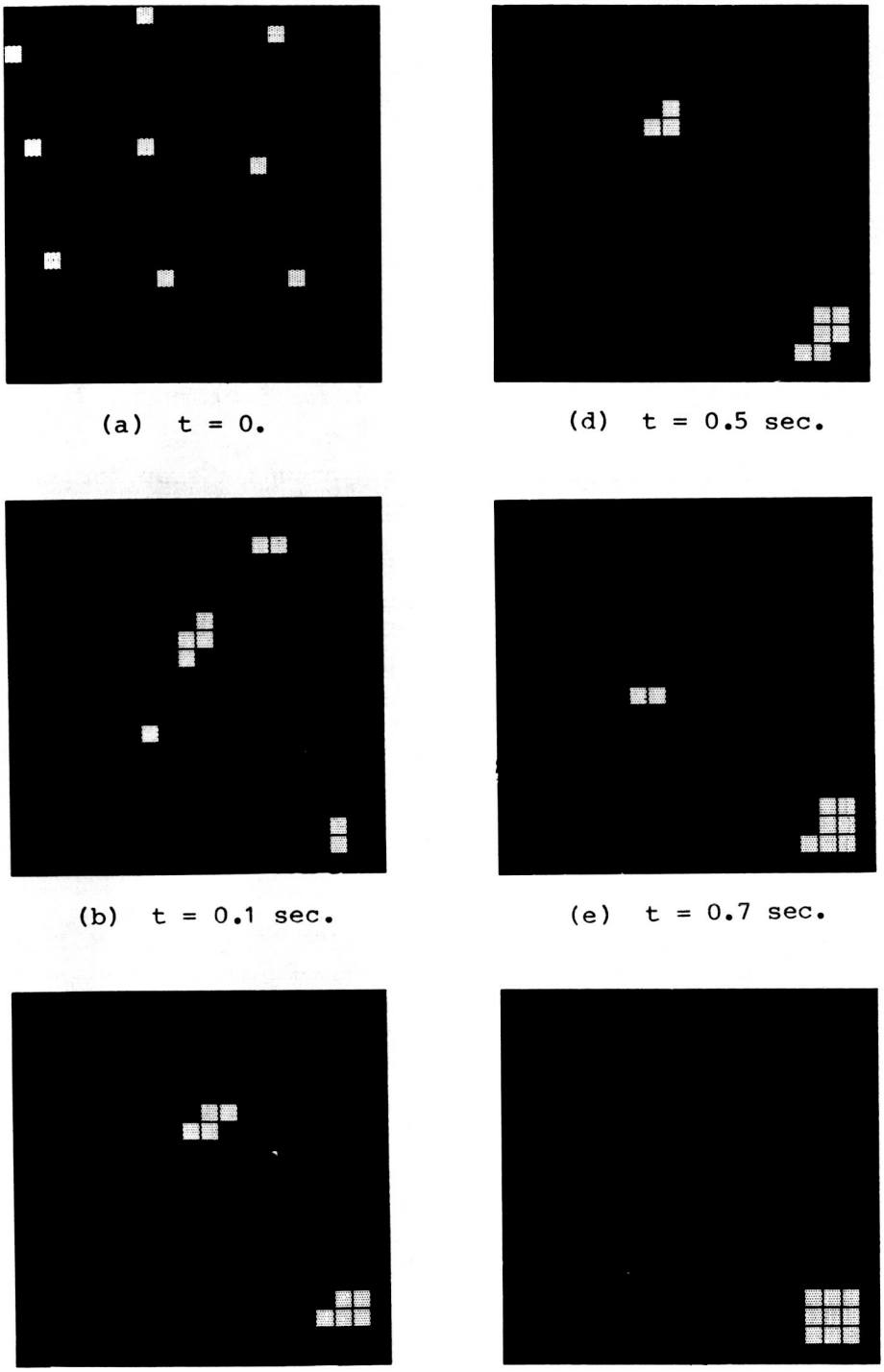

Figure 10.- Clustering of dispersed atoms on a uniform surface as a function of time. T = 600 K.

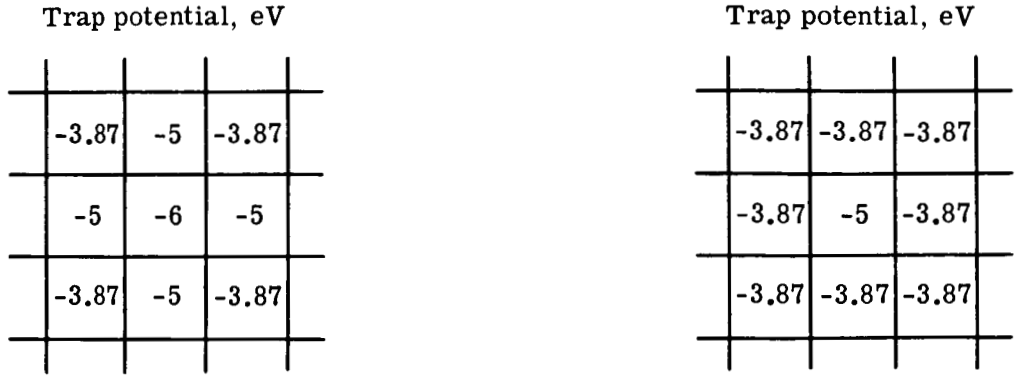

(a) First layer.

(b) Second layer.

Figure 11.- Variation in potential energy around a trap for first and second layers within the 400-site array.

around the site is shown in figure 12 for a constant deposition rate $R_d = 5 \times 10^{14}$ cm^{-2}-sec^{-1} and a substrate temperature $T = 550$ K. (Lighter shading of some of the SOS squares represents the next adlayer of the growing film.) As atoms impinge on the surface, heterogeneous nucleation occurs, and growth is so rapid in this vicinity that captured adatoms cause a depletion zone around the growing cluster. Further, the vertical growth rate is also larger than normal because the potential energy at the trap sites is still lower on the surface of the growing island than on the uniform-surface sites, thus generating the early growth of the second layer. It is therefore likely that growth in the vicinity of such a site would be dominated by this defect.

It has recently been observed that epitaxial growth is extremely sensitive to surface defect density and to the magnitude of the deposition rate (refs. 10 and 11). Growths have been achieved at very low temperatures on appropriate substrates only when the surface was relatively smooth and defect free (as determined by Kikuchi lines present in the reflection high-energy electron diffraction patterns). If the defect density is too high, then epitaxy is inhibited by the dominance of growth affected by the defects. If the deposition rate is too high, then even with low defect density the growth around the defects is so rapid that epitaxy is also limited. Therefore, an understanding of the growth rate about different types of defects, as well as a knowledge of the overall surface defect density, would be helpful in assessing the probability of epitaxy for a given system.

Experiment 4 - Thin-Film Growth With Variable Deposition Rate and Substrate Temperature

The representation of the growth for four different deposition rates over the temperature range 300 K to 600 K is presented in figures 13 to 16. The sequences in figure 13 show the dramatic difference in the growth of clusters due to the higher

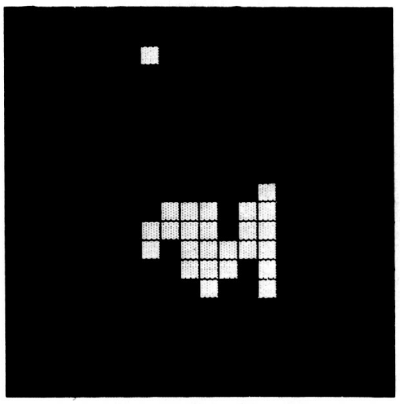

(a) t = 0.5 sec.

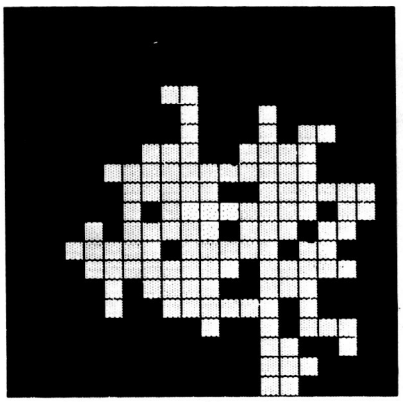

(d) t = 1.4 sec.

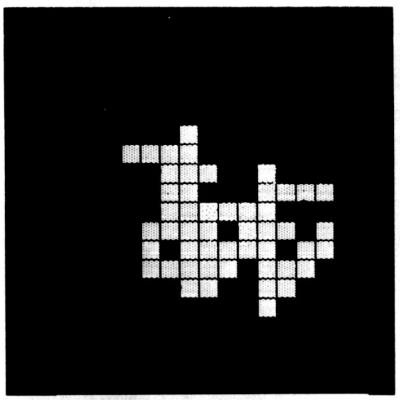

(b) t = 0.8 sec.

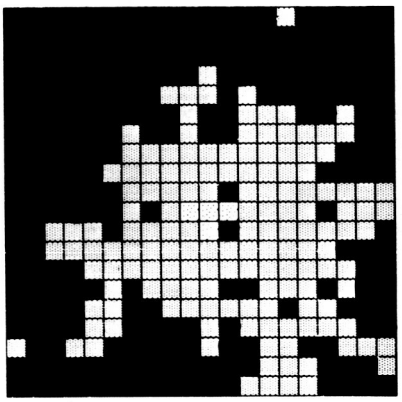

(e) t = 1.7 sec.

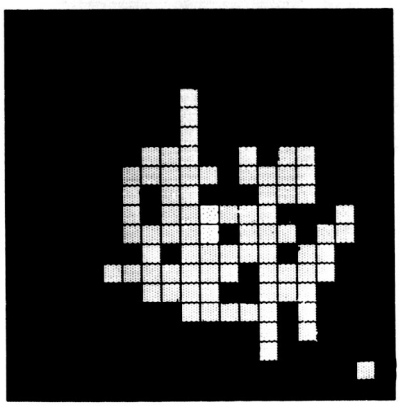

(c) t = 1.1 sec.

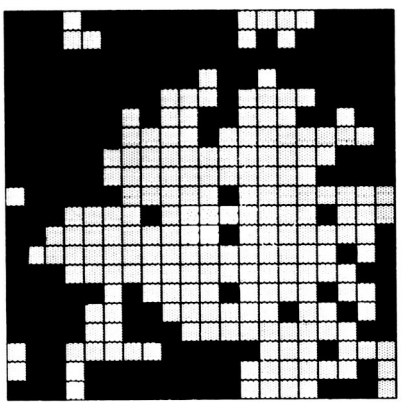

(f) t = 2.0 sec.

Figure 12.- Growth around trap. Lighter shading of SOS squares represents next adsorption layer of growing film. T = 550 K.

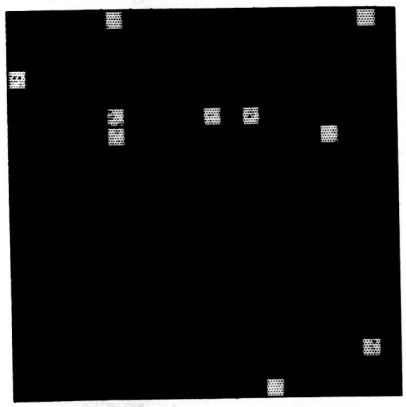

(a) T = 300 K; t = 0.5 sec.

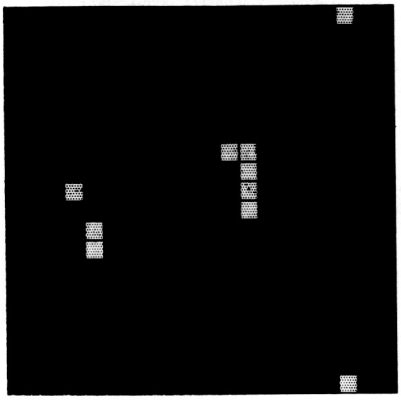

(d) T = 400 K; t = 0.5 sec.

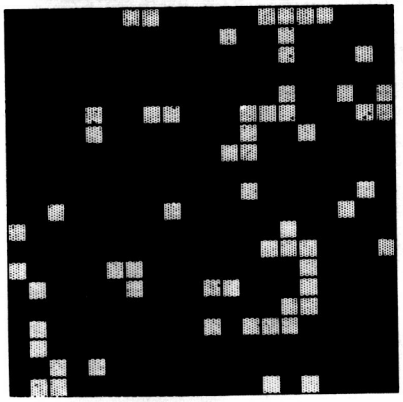

(b) T = 300 K; t = 3.0 sec.

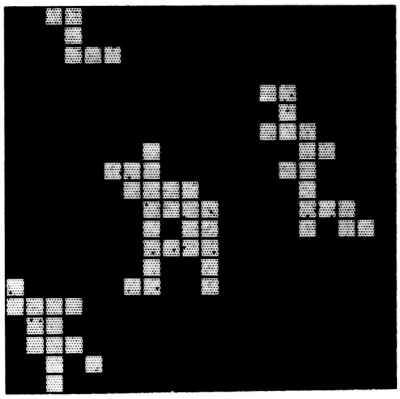

(e) T = 400 K; t = 3.0 sec.

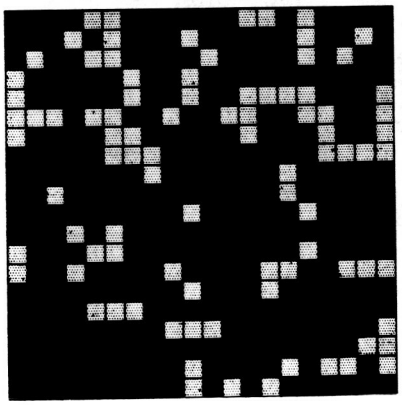

(c) T = 300 K; t = 6.0 sec.

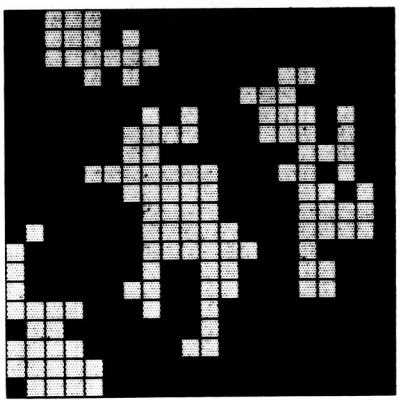

(f) T = 400 K; t = 6.0 sec.

Figure 13.- Deposition at $R_d = 5 \times 10^{13}$ cm^{-2}-sec^{-1}.

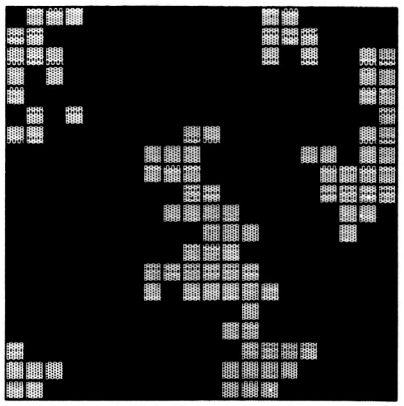

(a) t = 0.5 sec.

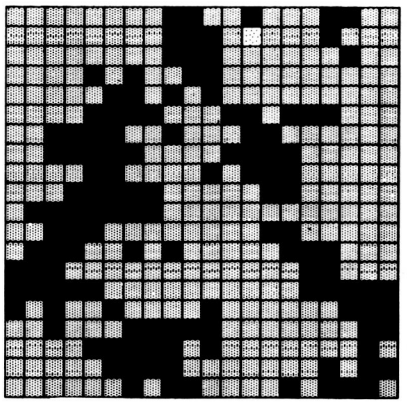

(d) t = 1.4 sec.

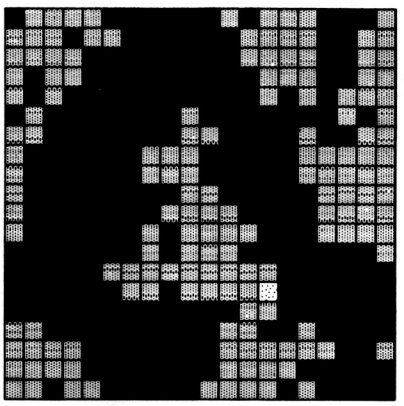

(b) t = 0.8 sec.

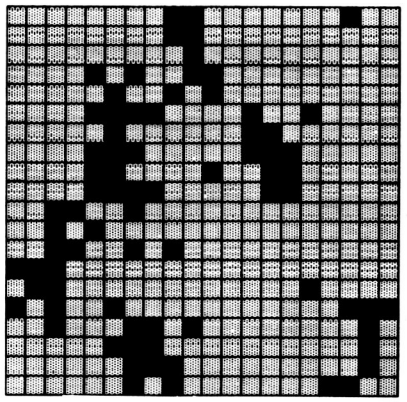

(e) t = 1.7 sec.

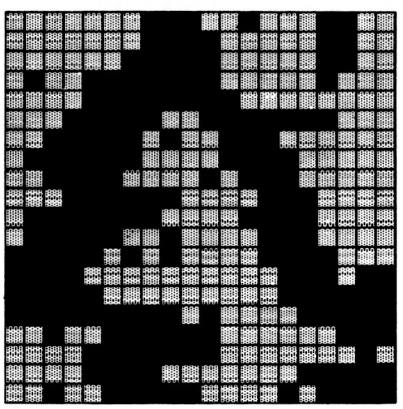

(c) t = 1.1 sec.

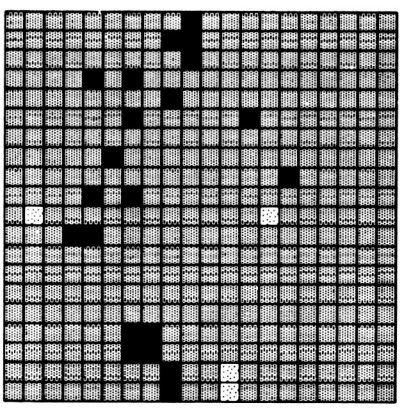

(f) t = 2.0 sec.

Figure 14.- Deposition at $R_d = 5 \times 10^{14}$ cm^{-2}-sec^{-1}. Lighter shading of SOS squares represents next adsorption layer of growing film. T = 500 K.

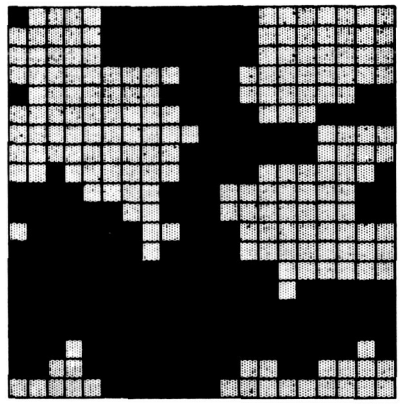

(a) t = 0.5 sec.

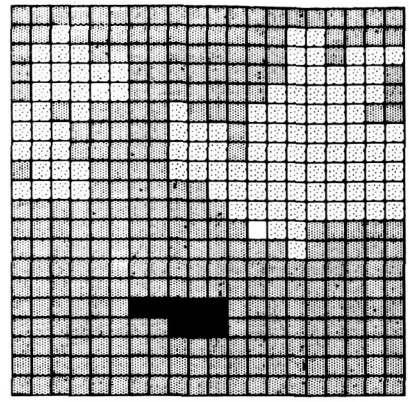

(d) t = 1.4 sec.

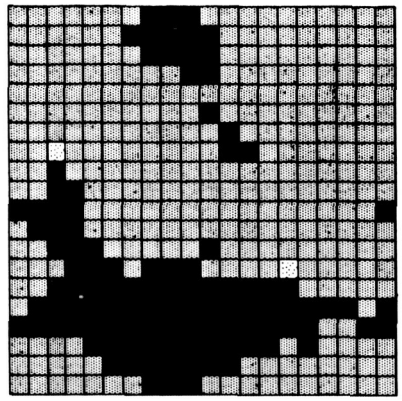

(b) t = 0.8 sec.

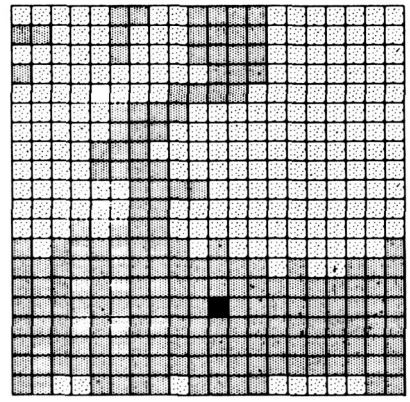

(e) t = 1.7 sec.

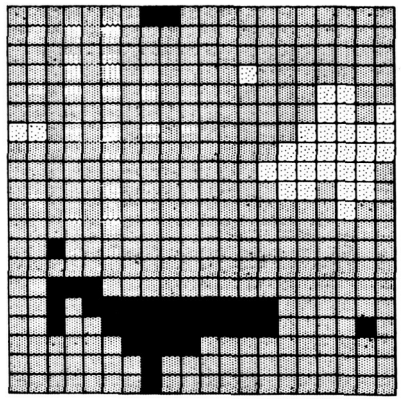

(c) t = 1.1 sec.

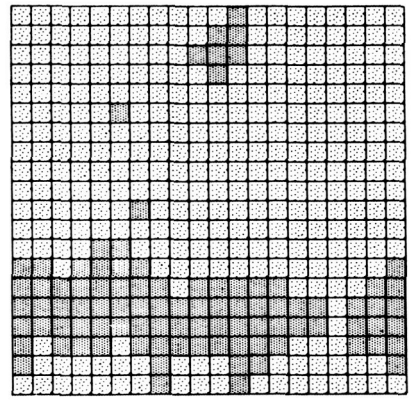

(f) t = 2.0 sec.

Figure 15.- Deposition at $R_d = 1 \times 10^{15}$ cm^{-2}-sec^{-1}. Lighter shading of SOS squares represents next adsorption layer of growing film. T = 600 K.

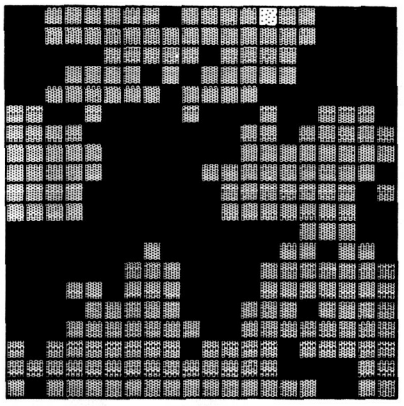

(a) t = 0.25 sec.

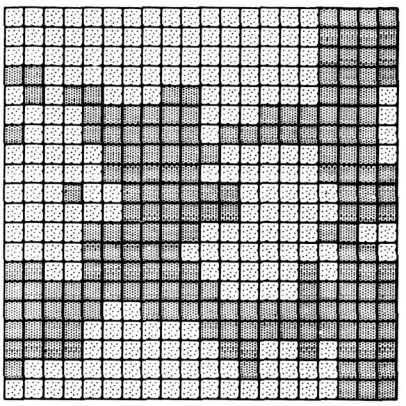

(d) t = 0.70 sec.

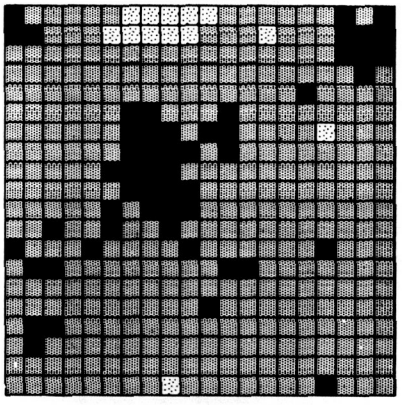

(b) t = 0.40 sec.

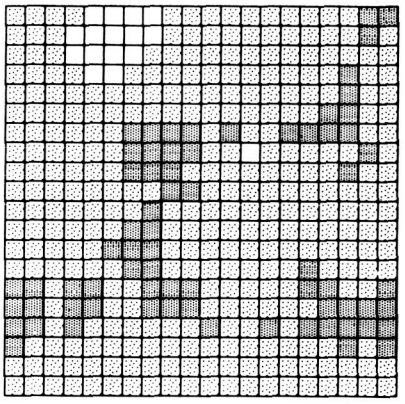

(e) t = 0.85 sec.

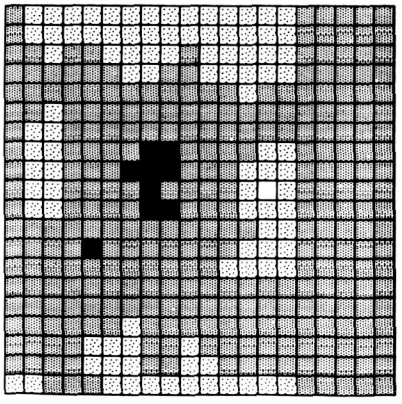

(c) t = 0.55 sec.

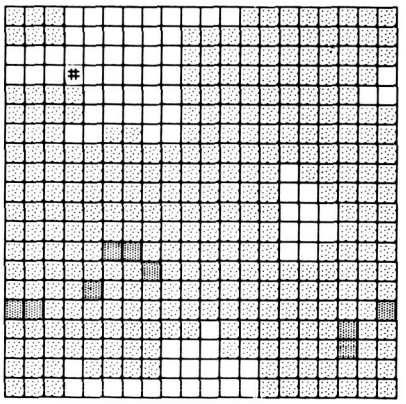

(f) t = 1.00 sec.

Figure 16.- Deposition at $R_d = 2.5 \times 10^{15}$ cm^{-2}-sec^{-1}. Lighter shading of SOS squares represents next adsorption layer of growing film. T = 600 K.

substrate temperature. This is simply a manifestation of the higher mobility of surface atoms. The growth of single clusters and their ultimate coalescence is shown in figure 14. This figure illustrates the development of a possible grain boundary. Although graphic representation of different growing grain orientations is not easily achieved with the SOS approach, the potential field surrounding a particular defect or nucleation site does provide some information about the probable growth orientation, and this may be sufficient to determine if the coalescing grains will be in or near registry (i.e., there will be a low-angle grain boundary) or whether a high-angle grain boundary will be formed.

Figure 15 shows the growth sequence that occurred when an advancing ledge was formed upon the coalescence of two large clusters. This behavior has also been observed by Weeks and Gilmer for calculated crystal growth from the melt (ref. 5). The sequence in figure 16 shows rapid growth; in only 1 second, the first layer is complete, the second layer is almost complete, the third layer has a large cluster, and there is even one adatom beginning the fourth layer.

The roughness factor as a function of time for these growths is presented in figures 17 and 18, and provides an indication of the changing surface uniformity. The roughness factor is given by $r = A/A_s$, where A and A_s are the surface areas of the growing film and the homogeneous substrate. The oscillating structure of the curves is a manifestation of the growing multilayers and the subsequent surface migration filling in the vacancies and the ledge and kink sites. At higher substrate temperatures, the more mobile adatoms fill in these sites faster; this tends to smooth out any structure in these curves.

A plot of cluster density n_s and cluster size N as a function of time is presented in figure 19 for a deposition rate of 5×10^{14} cm^{-2}-sec^{-1}. Clusters of size n_i $(i > 1)$ have a total density of

$$\sum_{i=2}^{\infty} n_i = n_s \tag{23}$$

Definite maxima in these curves are observed for all temperatures tested. As is apparent from figures 13 to 16, the decay in n_s is due to the coalescence of the clusters. This behavior has also been observed by Donohoe and Robins for Ag/NaCl (ref. 12), Hamilton and Logel for Ag/C and Pd/C (ref. 13), and Corbett and Boswell for Ag/MoS_2 (ref. 14). The maximum cluster size also decreases with increasing temperature, as was observed by Poppa for Bi/C and Ag/C (ref. 15). The most probable size of the clusters for the maxima at $T = 300$ K and $t = 5.5$ sec is approximately two to three atoms.

The initial slope of the n_s curves in figure 19 gives the nucleation rate (ref. 16)

$$J_o = Z\sigma^*(R\tau_o)^{i^*+1} \exp\left[\frac{E_{i^*} + (i^* + 1)\Delta H_{ads} - Q_d}{kT}\right] \tag{24}$$

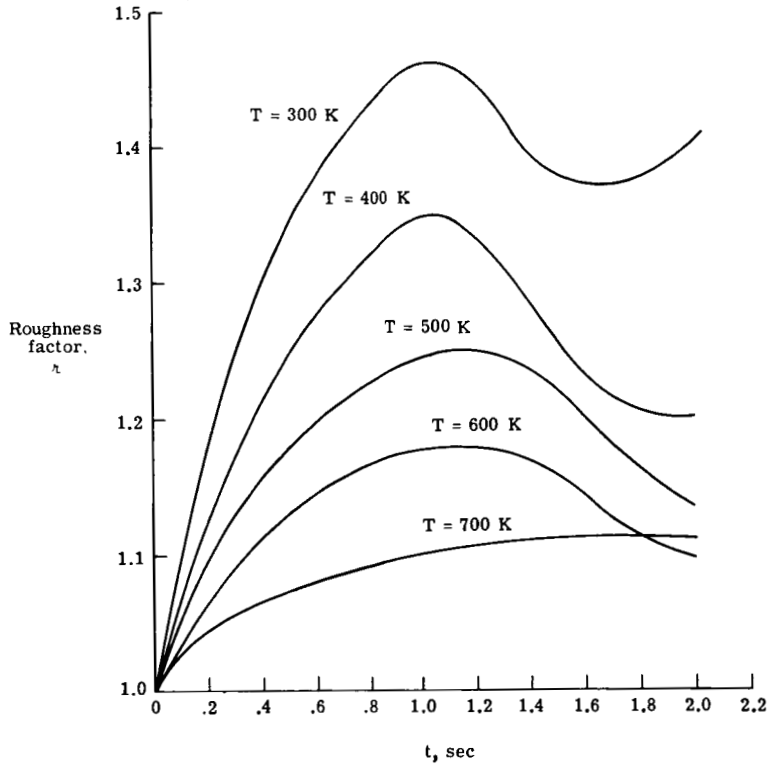

Figure 17.- Surface roughness factor for $R_d = 5 \times 10^{14}$ cm^{-2}-sec^{-1} and several temperatures. Completed layers correspond to minima in curves.

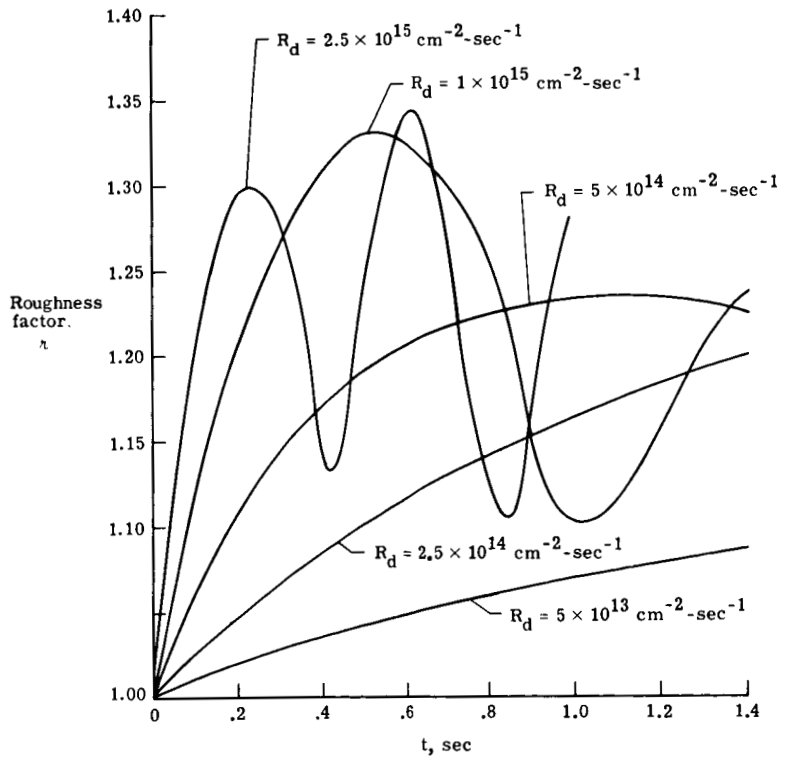

Figure 18.- Surface roughness factor at T = 500 K for several deposition rates.

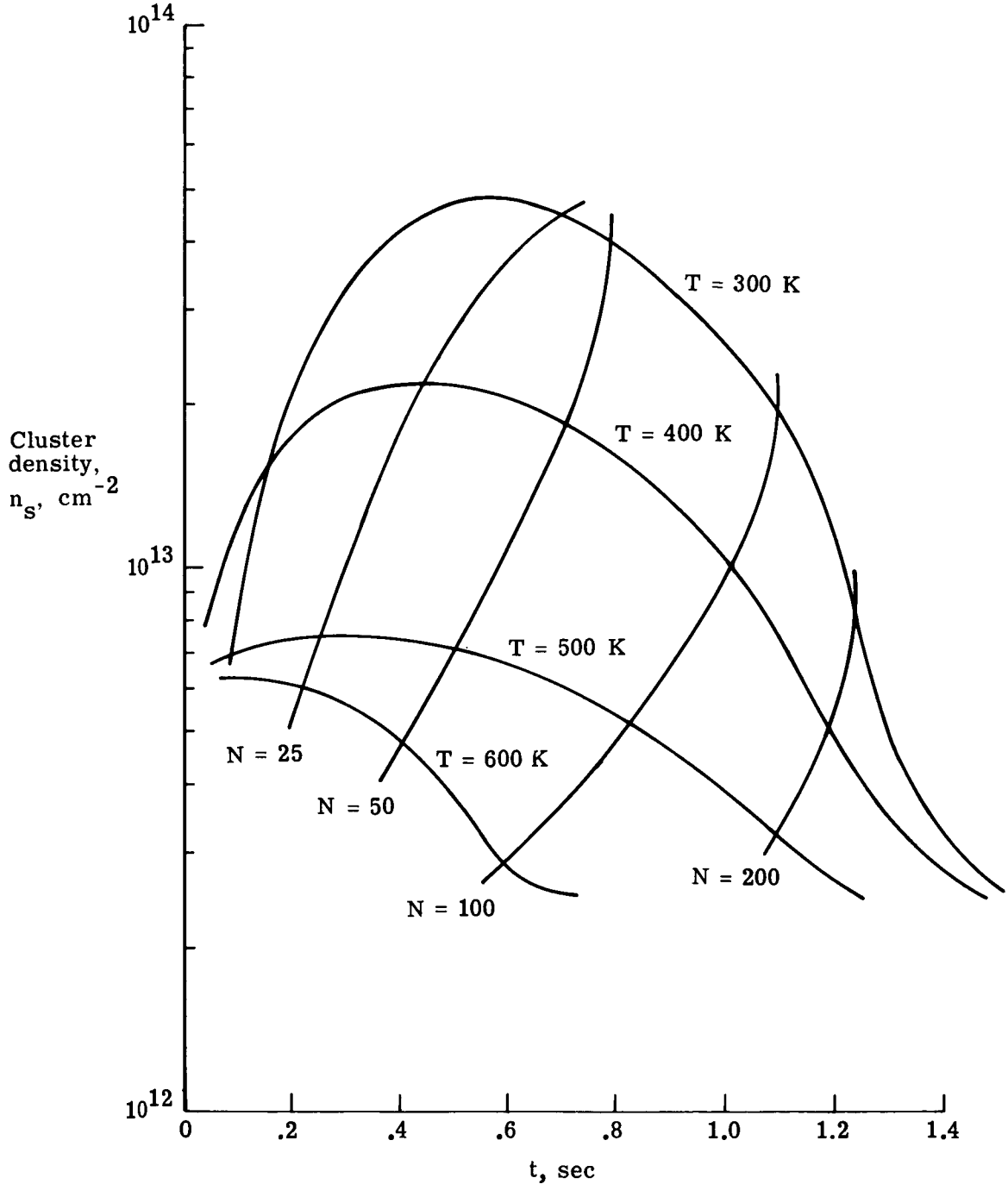

Figure 19.- Cluster density n_s as function of time with constant-cluster curves for 25, 50, 100, and 200 atoms. Decrease in n_s corresponds to growth coalescence. $R_d = 5 \times 10^{14}$ cm^{-2}-sec^{-1}.

where Z is the Zeldovitch factor, σ^* is the capture number, E_{i^*} is the cluster energy, and i^* is the critical nucleus size. If it is assumed in this case that $Z\sigma^* = 1$ and $i^* = 1$, then

$$\frac{J_{o1}}{R_{d1}^2} = \frac{J_{o2}}{R_{d2}^2}$$

At $T = 300$ K, the model gives

$$J_o/R_d^2 = 2.93 \times 10^{-15} \text{ cm}^2\text{-sec} \qquad (R_d = 5 \times 10^{13} \text{ cm}^{-2}\text{-sec}^{-1})$$

$$J_o/R_d^2 = 2.67 \times 10^{-15} \text{ cm}^2\text{-sec} \qquad (R_d = 5 \times 10^{14} \text{ cm}^{-2}\text{-sec}^{-1})$$

and at $T = 400$ K, the model gives

$$J_o/R_d^2 = 8.7 \times 10^{-16} \text{ cm}^2\text{-sec} \qquad (R_d = 5 \times 10^{13} \text{ cm}^{-2}\text{-sec}^{-1})$$

$$J_o/R_d^2 = 7.9 \times 10^{-16} \text{ cm}^2\text{-sec} \qquad (R_d = 5 \times 10^{14} \text{ cm}^{-2}\text{-sec}^{-1})$$

This is reasonably good agreement, and indicates that the critical nucleus is indeed $i^* = 1$.

Experiment 5 - Annealing of Thin-Film Growth

Annealing of a given deposition or growth proceeds by surface diffusion or monomer exchange between clusters (Ostwald ripening). As discussed previously, cluster peripheral motion can also occur causing an increase in the order of the growth. Figure 20(a) shows the initial growth condition $R_d = 5 \times 10^{13}$ cm^{-2}-sec^{-1} when $T = 300$ K. The temporal variation in growth rate for $R_d = 0$ with the substrate temperature increased to 600 K and then to 700 K is presented in figures 20(b) through 20(e). For both temperatures, each island or cluster is driven to the more ordered arrangements shown and the number of smaller nuclei has noticeably decreased for the longer elapsed time. Figure 21 shows the effect of temperature on the average density of the clusters. This same sort of linear decrease in the cluster density was found by Donohoe and Robins for the system Au/NaCl (ref. 12). Annealing at deposition temperature did not seem to have a significant effect on cluster density even for large times, but when the temperature was increased, the low-density clusters ultimately broke up by monomer exchange to the larger, more stable clusters.

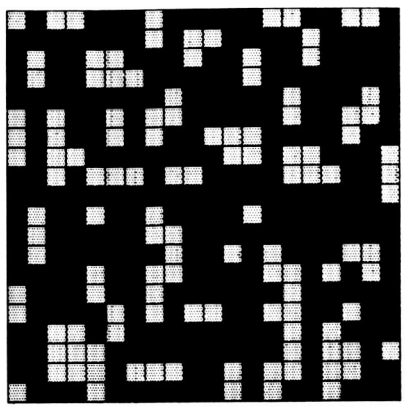

(a) $R_d = 5 \times 10^{13}$ cm^{-2}-sec^{-1};
T = 300 K; t = 0 sec.

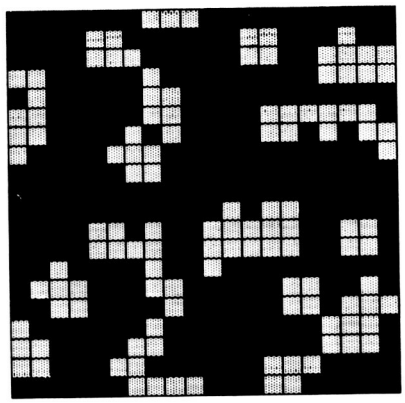

(b) $R_d = 0$; T = 600 K;
t = 3.0 sec.

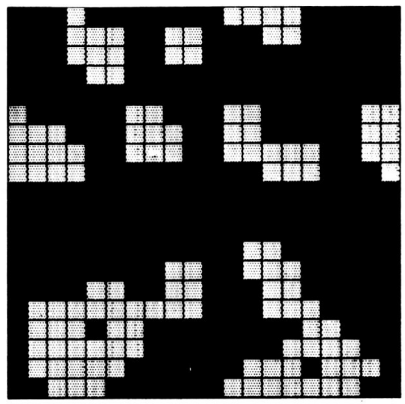

(d) $R_d = 0$; T = 700 K;
t = 3.0 sec.

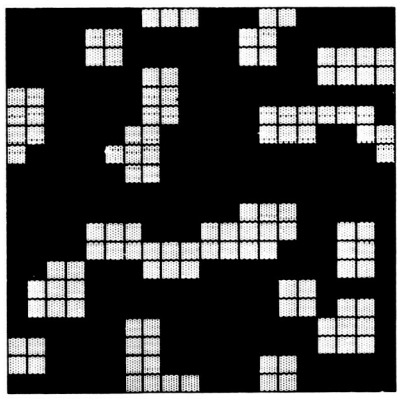

(c) $R_d = 0$; T = 600 K;
t = 6.0 sec.

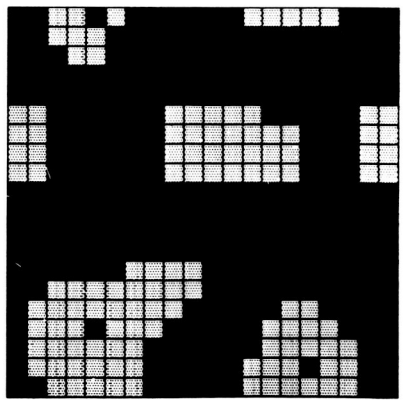

(e) $R_d = 0$; T = 700 K;
t = 6.0 sec.

Figure 20.- Annealing of deposition.

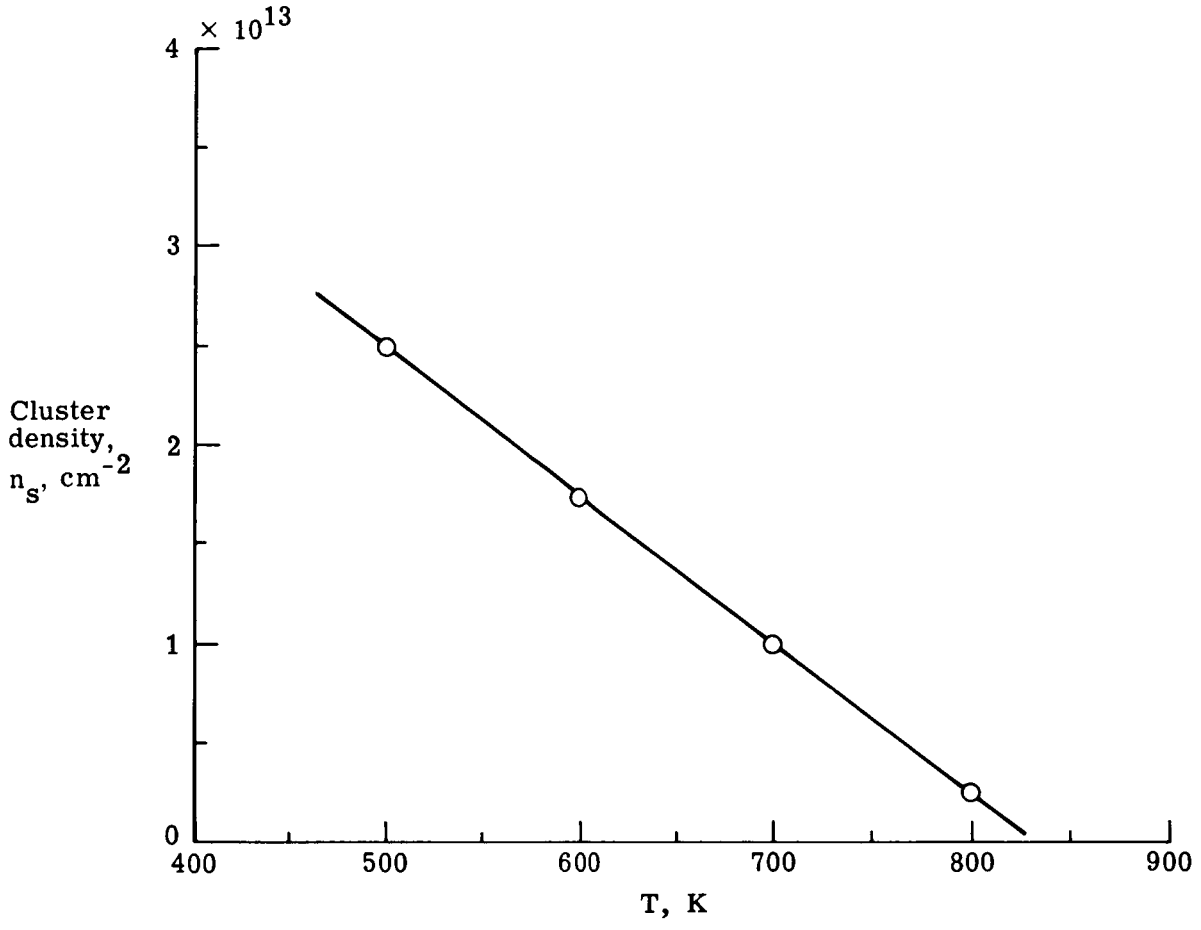

Figure 21.- Annealing effects on cluster size. $(n_s)_{T=300} = 7.75 \times 10^{13}$ cm^{-2}; t = 6 sec; $\theta = 0.3$.

CONCLUDING REMARKS

A solid-on-solid (SOS) Monte Carlo computer simulation utilizing a potential-energy scaling technique has been used to model the initial stages of thin-film growth. The method employs Boltzmann-ordered statistics to simulate fluctuations in vibrational energy at each site in the 20 × 20 array. Subsequent events of adsorption, desorption, surface migration, incorporation, and substrate atom diffusion to the surface are considered, and their effect on the potential-energy field at each site is continually updated and recorded. The results of several computer experiments show consistency with the expected behavior of thin-film growth. Surface migration data taken at different substrate temperatures verified the activation energy as determined by an Arrhenius plot. Dispersed adatoms were observed to cluster into dimers and trimers and finally to form a single cluster in its most stable configuration. A point defect was designed by varying the interaction potential in the lateral (x,y) and vertical (z) directions, and served to illustrate the preferred growth that is known to occur at such defects. This procedure appears to be a promising approach in the study of such defects. Experiments with varying deposition rate and substrate temperature showed the expected behavior of thin-film growth, from

nucleation and cluster growth to coalescence. The nucleation rate was found to be proportional to the square of the deposition rate, in agreement with the atomistic theory of nucleation. Finally, annealing experiments demonstrated the ordering of clusters as a function of time and temperature.

Langley Research Center
National Aeronautics and Space Administration
Hampton, VA 23665
December 2, 1982

REFERENCES

1. Moon, R. L.; James, L. W.; Locker, D. R.; Rahilly, W. P.; Lowe, L.; and Mees, J. M.: Performance of AlGaAs/GaAs Solar Cells in the Space Environment. Conference Record of the Twelfth IEEE Photovoltaic Specialists Conference - 1976, 76CH1142-9 ED, IEEE, 1976, pp. 255-261.

2. Lewis, B.; and Anderson, J. C.: Nucleation and Growth of Thin Films. Academic Press, Inc., 1978.

3. Abraham, Farid F.; and White, George M.: Computer Simulation of Vapor Deposition on Two-Dimensional Lattices. J. Appl. Phys., vol. 41, no. 4, Mar. 15, 1970, pp. 1841-1849.

4. Van der Eerden, J. P.; Bennema, P.; and Cherepanova, T. A.: Survey of Monte Carlo Simulations of Crystal Surfaces and Crystal Growth. Progress in Crystal Growth and Characterization - Volume 1, Brian R. Pamplin, ed., Pergamon Press, Ltd., c.1978, pp. 219-254.

5. Weeks, John D.; and Gilmer, George H.: Dynamics of Crystal Growth. Advances in Chemical Physics - Volume XL, I. Prigogine and Stuart A. Rice, eds., John Wiley & Sons, Inc., c.1979, pp. 157-227.

6. Hogg, Robert V.; and Craig, Allen T.: Introduction to Mathematical Statistics, 3rd ed. Macmillan Pub. Co., Inc., c.1970.

7. Van Hove, M. A.: Surface Crystallography and Bonding. The Nature of the Surface Chemical Bond, T. N. Rhodin and G. Ertl, eds., North-Holland Pub. Co., c.1979, pp. 275-311.

8. Bonzel, H. P.: Transport of Matter at Surfaces. Surface Physics of Materials - Volume II, J. M. Blakely, ed., Academic Press, Inc., c.1975, pp. 279-338.

9. Crank, J.: The Mathematics of Diffusion. Oxford Univ. Press, 1956.

10. Prinz, G. A.; and Krebs, J. J.: Molecular Beam Epitaxial Growth of Single-Crystal Fe Films on GaAs. Appl. Phys. Lett., vol. 39, no. 5, Sept. 1, 1981, pp. 397-399.

11. Prinz, G. A.; and Ferrari, J. M.: Molecular Beam Epitaxial Growth of Single Crystal Aℓ Films on GaAs (110). Appl. Phys. Lett., vol. 40, no. 2, Jan. 15, 1982, pp. 155-157.

12. Donohoe, A. J.; and Robins, J. L.: Mobility and Coalescence of Nuclei in Metal Vapor Deposition on Alkali Halide Substrates. J. Cryst. Growth, vol. 17, Dec. 1972, pp. 70-76.

13. Hamilton, J. F.; and Logel, P. C.: Nucleation and Growth of Ag and Pd on Amorphous Carbon by Vapor Deposition. Thin Solid Films, vol. 16, no. 1, Apr. 1973, pp. 49-63.

14. Corbett, J. M.; and Boswell, F. W.: Experimental Investigation of the Nucleation of Silver on Molybdenite. J. Appl. Phys., vol. 40, no. 6, May 1969, pp. 2663-2669.

15. Poppa, Helmut: Heterogeneous Nucleation of Bi and Ag on Amorphous Substrates (In Situ Electron Microscopy Studies). J. Appl. Phys., vol. 38, no. 10, Sept. 1967, pp. 3883-3894.

16. Walton, D.: Nucleation of Vapor Deposits. J. Chem. Phys., vol. 37, no. 10, Nov. 15, 1962, pp. 2182-2188.

NOMENCLATURE

A	surface area of growing film, cm^2
A_s	surface area of homogeneous substrate, cm^2
a_o	interatomic distance, cm
c_b	bulk concentration, cm^{-3}
Δc_s	surface concentration, cm^{-2}
D	diffusion coefficient, cm^2-sec^{-1}
$E(i,j)$	total energy at site (i,j) on second and succeeding layers, eV
$E_s(i,j)$	total energy of surface layer at site (i,j), eV
E_{i*}	cluster energy, eV
$F(\varepsilon)$	cumulative distribution function, dimensionless
$f(\varepsilon)$	distribution function, dimensionless
$G(\varepsilon)$	cumulative ordered distribution function, dimensionless
$g(\varepsilon)$	ordered distribution function, dimensionless
ΔH_{ads}	heat of adsorption, eV
ΔH_{cl}	heat of sublimation from completed layer, eV
ΔH_{des}	heat of desorption, eV
$i*$	critical cluster size, dimensionless
J_o	nucleation rate, cm^{-2}-sec^{-1}
k	Boltzmann's constant, eV/K
ℓ	coordination number, dimensionless
N	cluster size, cm^{-2}
n	random sample number, dimensionless
n_i	cluster density of size i, cm^{-2}
n_s	cluster density (monomers excluded), cm^{-2}
P	statistical probability
Q_d	activation barrier for surface diffusion, eV
R	random number, dimensionless

R_d	deposition rate, $cm^{-2}sec^{-1}$
k	roughness factor
S	sticking coefficient, dimensionless
S_o	sticking coefficient at zero coverage, dimensionless
T	substrate temperature, K
t	time, sec
Δt_s	sampling time, sec
U(i,j)	potential energy at site (i,j), eV
U_i	threshold energy for incorporation, eV
U_m	threshold energy for migration, eV
U_o	potential energy at site (i,j) on uniform surface, eV
x,y,z	coordinate system relative to film surface, cm
Z	Zeldovitch factor, dimensionless
α	incremental energy change, nearest neighbor, eV
β	incremental energy change, second-nearest neighbor, eV
γ	incremental energy change, third-nearest neighbor, eV
δ	thickness of film, cm
ε	random vibrational energy, eV
ε_o	maximum random vibrational energy, eV
$\varepsilon_{(n)}$	vibrational energy from ordered statistics, eV
η	number of bonds, dimensionless
θ	coverage, dimensionless
λ	inverse energy, eV^{-1}
ν_{des}	desorption flux, cm^{-2}-sec^{-1}
ξ	order of bonding
σ^*	cluster capture number, dimensionless
τ	stay time, sec

τ_d average mean time between hops

τ_o vibrational period, sec

ϕ single-bond energy, eV

ϕ_o energy change at adsorption site, eV

1. Report No.	2. Government Accession No.	3. Recipient's Catalog No.
NASA TP-2102		

4. Title and Subtitle	5. Report Date
A POTENTIAL-ENERGY SCALING MODEL TO SIMULATE THE INITIAL STAGES OF THIN-FILM GROWTH	February 1983
	6. Performing Organization Code 506-55-43-01
7. Author(s) J. H. Heinbockel, R. A. Outlaw, and G. H. Walker	8. Performing Organization Report No. L-15531
	10. Work Unit No.
9. Performing Organization Name and Address NASA Langley Research Center Hampton, VA 23665	11. Contract or Grant No.
	13. Type of Report and Period Covered Technical Paper
12. Sponsoring Agency Name and Address National Aeronautics and Space Administration Washington, DC 20546	14. Sponsoring Agency Code

15. Supplementary Notes

J. H. Heinbockel: Old Dominion University, Norfolk, Virginia.
R. A. Outlaw and G. H. Walker: Langley Research Center.

16. Abstract

A solid-on-solid (SOS) Monte Carlo computer simulation employing a potential-energy scaling technique has been used to model the initial stages of thin-film growth. The model monitors variations in the vertical interaction potential that occur due to the arrival or departure of selected adatoms or impurities at all sites in the 20 × 20 array. Boltzmann-ordered statistics are used to simulate fluctuations in vibrational energy at each site in the array, and the resulting site energy is compared with threshold levels of possible atomic events. In addition to adsorption, desorption, and surface migration, adatom incorporation and diffusion of a substrate atom to the surface are also included. The lateral interaction of nearest, second-nearest, and third-nearest neighbors is also considered. A series of computer experiments are conducted to illustrate the behavior of the model.

17. Key Words (Suggested by Author(s))	18. Distribution Statement
Thin films Nucleation and growth Monte Carlo simulation Epitaxy	Unclassified - Unlimited Subject Category 26

19. Security Classif. (of this report)	20. Security Classif. (of this page)	21. No. of Pages	22. Price
Unclassified	Unclassified	36	A03

For sale by the National Technical Information Service, Springfield, Virginia 22161

NASA-Langley, 1983